Inversion of Fault Zone Properties Using Dynamic Data

Z. A. Reza (zreza@ualberta.ca) and C. V. Deutsch (cdeutsch@civil.ualberta.ca)
Department of Civil & Environmental Engineering, University of Alberta

X. H. Wen (xwen@chevrontexaco.com)
ChevronTexaco Exploration and Production Technology Company

Abstract

Reservoir heterogeneity has a large effect on performance of a reservoir. Faults may act as barriers creating compartmentalized reservoirs or as high conductivity conduits in an otherwise tight reservoir system. Often, the location of such faults or fault zones are identified with seismic data; however, the conductive characteristics of the fault zones cannot be resolved with seismic. We develop an inversion algorithm for fault zone transmissibility characterization using multiple well production data. This is an extension of simultaneous porosity and permeability inversion using a modified Sequential Self-Calibration (SSC) method.

Introduction

Reservoir heterogeneity has a large effect on performance of a reservoir. Faults may act as barriers creating compartmentalized reservoirs or as high conductivity conduits in an otherwise tight reservoir system. Often, the location of such faults or fault zones are identified with seismic data; however, the conductive characteristics of the fault zones cannot be resolved with seismics. Faults may affect the dynamic flow responses of the reservoir system. We develop an inversion algorithm for fault zone permeability characterization using multiple well flow response data.

Algorithm Description

An algorithm for simultaneous inversion of porosity and permeability was developed using a modified SSC method [1]. Here, we extend the algorithm for fault zone permeability characterization.

The basic approach of sensitivity computation remains the same. Some master points are assigned for fault zone cells. The properties (porosity and permeability) in these cells are optimized in the same inner optimization loop with the other master points for unfaulted zones. The optimal corrections for regular grid cells are propagated as before; however, the fault zone properties are taken as averages for each fault and kept constant for every cell representing the fault.

Thus, a methodology has been developed for simultaneous inversion of porosity and permeability. The steps involved in this extended algorithm follow.

1. Select regular master points and fault zone master points.
2. Perform Steps (2) to (9) involved in simultaneous inversion algorithm discussed in [1].
3. Determine and assign the weighted averaged optimal corrections to fault blocks.
4. Update initial ϕ and y fields.
5. Repeat Steps (1) to (4) till convergence is achieved.

The salient idea of this algorithm is to isolate the domains - the faulted ones and the unfaulted reservoir domain. Separate collection of master points and the constraint sets are set up for the respective domains. Propagation of optimal master point corrections are performed within the

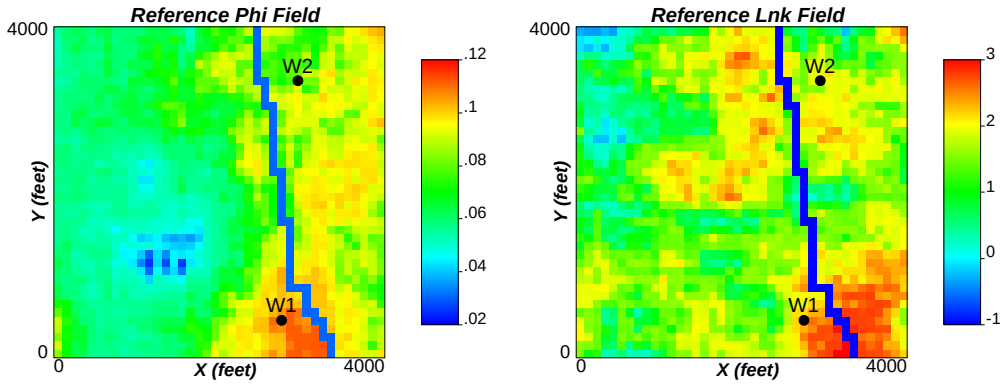

Figure 1: Reference faulted ϕ and $\ln(k)$ fields: Sealing Fault Example (Case A).

faulted domains by some averaging scheme, whereas for the unfaulted reservoir domain through kriging weights.

In the following sections, we demonstrate the ability of the code to retrieve fault zone properties with some synthetic examples. First, we discuss a sealing fault example with only two wells. We investigate the dependence of the well locations with respect to the fault. In one case, the wells are in the opposite side of the fault, while in the other they are in the same side of the faults. Then, we perform the inversion of a faulted reservoir with high permeability fault with similar two-well cases. Finally, some sensitivity studies on the inversion process are performed.

Sealing Fault Example

A synthetic realistic example is demonstrated here to evaluate the ability of the algorithm to characterize fault zone permeabilities from multiple well production data. Faulted reference porosity and permeability fields are constructed first. Dynamic pressure responses at a number of wells are obtained by flow simulation.

Case A: 2 Wells on the Opposite Side of the Fault

A 2D 4000-ft square domain is discretized into 40 $\times$ 40 grid cells of 100 $\times$ 100 ft. Porosity and permeability fields are shown in Figure 1. There are 2 wells: Well W1 at the center of the cell (28,5), and Well W2 is at (30,34) (shown in Figure 1). The boundaries on all four sides are no-flow boundaries. Reservoir thickness is 100 ft, viscosity is 0.2 cp, formation compressibility 10^{-6} psi^{-1}, and well radius 0.3 ft. Figure 2 shows the imposed production rates and the corresponding numerically simulated pressure responses at the two wells. The histogram and the scatter-plot between ϕ and $\ln(k)$ are shown in Figures 3 and 4, respectively. Mean and standard deviation of reference distributions are 0.071 and 0.019 for ϕ, and 1.293 and 1.277 for $\ln(k)$. The low average porosity confirms the low storativity of the reservoir. The correlation coefficient between porosity and permeability is 0.541. A fault extends across the reservoir dividing the reservoir in two separate compartments with one having relatively higher porosity and permeability. The fault is acting as a flow barrier with poor fault zone petrophysical properties. The reference fault zone porosity and $\ln(k)$ are 0.03 and -5.0. Despite the simplicity of this example, inversion of these fault zone properties can be extremely difficult using multiple well production data. The reason for difficulty is the fact that subsurface flow is diffusive in nature. The effect of fault zones or narrow streak of abnormal properties may be masked by an effective ensemble properties in the region. In other words, both the scenarios of the effective homogenized properties and the fault zones may give rise to similar pressure profile for given flow rates.

Static well data are shown in Figure 5. Inversion was performed using 5 $\times$ 5 (=25) master points for reservoir models and 8 master points for fault properties. The prior variogram models used in

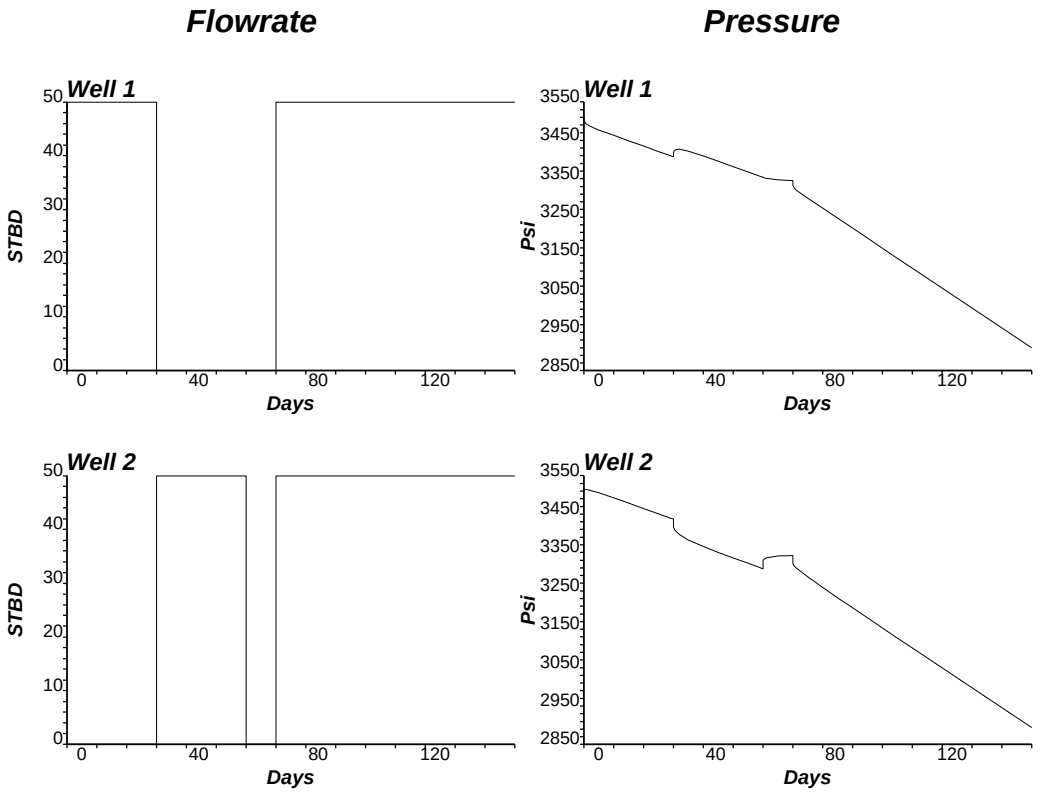

Figure 2: Production data (pressure and flow rates) obtained for 2 wells from the reference field: Sealing Fault Example (Case A).

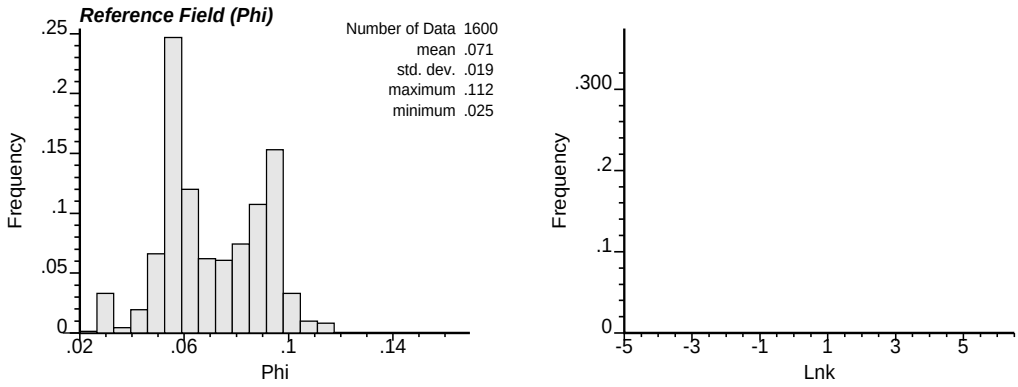

Figure 3: Histograms of reference ϕ and $\ln(k)$ fields: Sealing Fault Example (Case A).

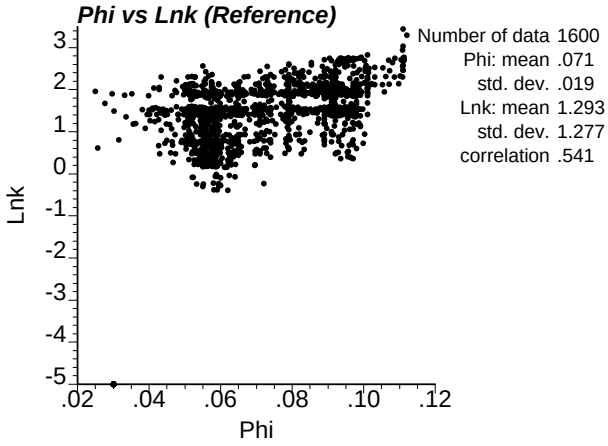

Figure 4: Scatterplot of reference ϕ and $\ln(k)$ distributions: Sealing Fault Example (Case A).

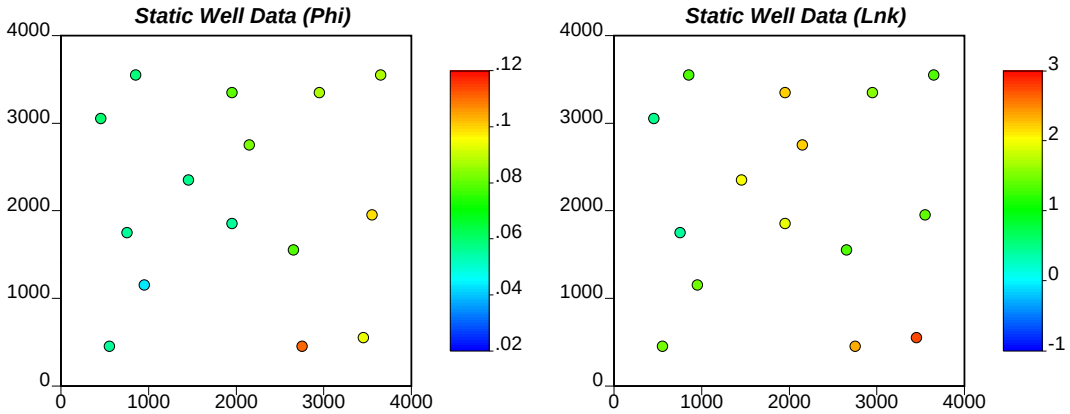

Figure 5: Static well data for ϕ and $\ln(k)$: Fault Property Inversion.

this run for ϕ and $\ln(k)$ are given in Equations 1 and 2:

$$\gamma_\phi(h) = 0.0 + 0.4Sph(h)\begin{matrix} a_x = 1000 \\ a_y = 3000 \end{matrix} + 0.6Sph(h)\begin{matrix} a_x = 9000 \\ a_y = 4000 \end{matrix} \tag{1}$$

and

$$\gamma_y(h) = 0.0 + 0.35Sph(h)\begin{matrix} a_x = 1000 \\ a_y = 3000 \end{matrix} + 0.65Sph(h)\begin{matrix} a_x = 8000 \\ a_y = 4500 \end{matrix} . \tag{2}$$

The inverted models are obtained after 70 outer iterations (18.5 minutes in a 1.8 GHz processor personal computer). The pressure responses in the updated porosity and permeability fields converge to the reference pressure data. These inverted models are shown in Figure 6. Figure 7 shows the pressure values at the ten wells computed from the true (from reference), initial and final updated porosity and permeability fields. Final pressure match is remarkable. Final average pressure mismatch (in L^2 norm sense) was only 2.527 psi. The objective function values of the inversion process are shown in Figure 8. The fault zone properties at all outer iterations are shown in Figures 9 and 10 for porosity and permeability values. Updated porosity and permeability fields at some outer iterations of the inversion method are shown in Figures 11 and 12.

Case B: 2 Wells in the Same Side of the Fault

The 2 wells are now on the same side of the faults: Well W1 at the center of the cell (28,5), and Well W2 is at (20,34). The wells are shown in Figure 13. Other information and parameters are

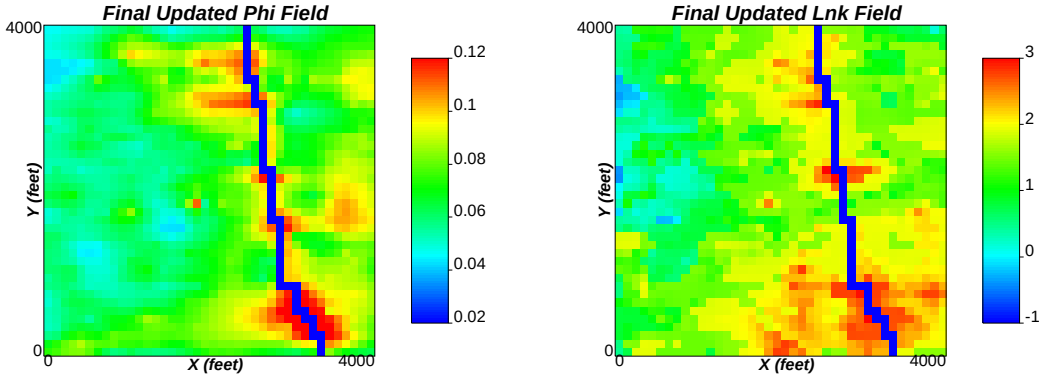

Figure 6: Updated ϕ and $\ln(k)$ fields: Sealing Fault Example (Case A).

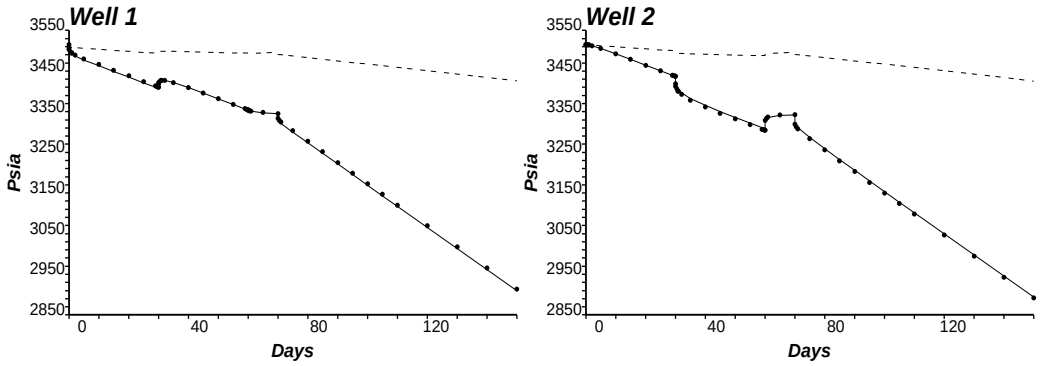

Figure 7: Pressure responses computed from initial (dashed lines) and updated (bullets) ϕ and $\ln(k)$ fields with the true data (solid lines): Sealing Fault Example (Case A).

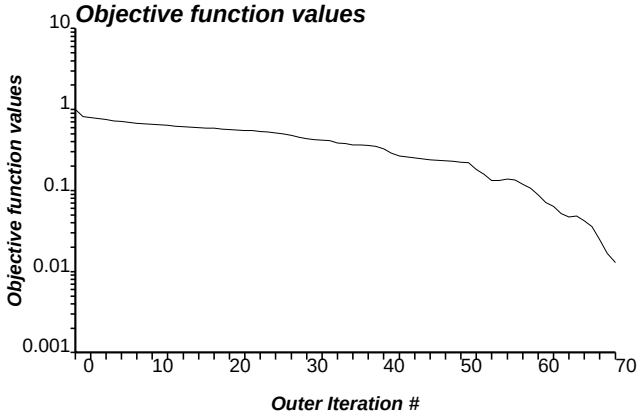

Figure 8: Objective function values of the inversion process: Sealing Fault Example (Case A).

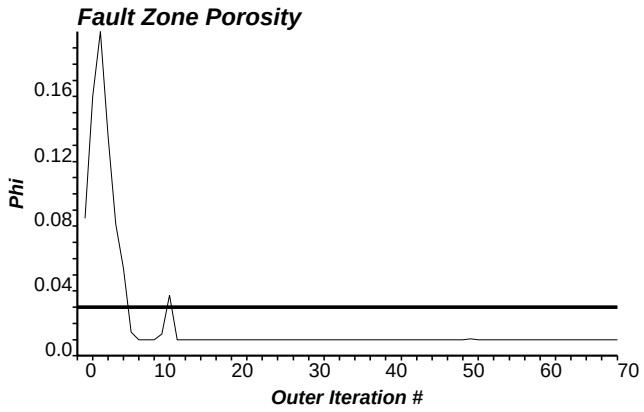

Figure 9: Fault zone ϕ values at each outer iteration: Sealing Fault Example (Case A). (Reference value: thicker horizontal line)

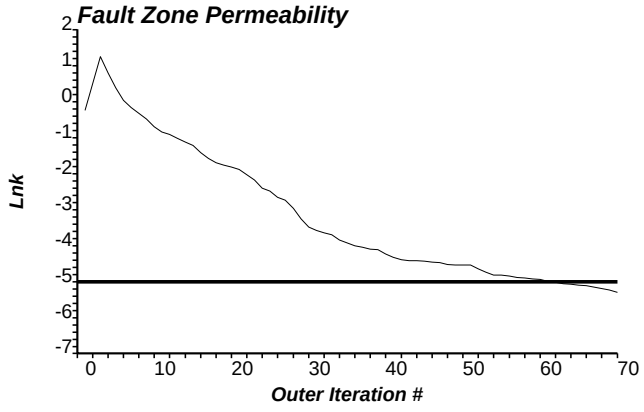

Figure 10: Fault zone $\ln(k)$ values at each outer iteration: Sealing Fault Example (Case A). (Reference value: thicker horizontal line)

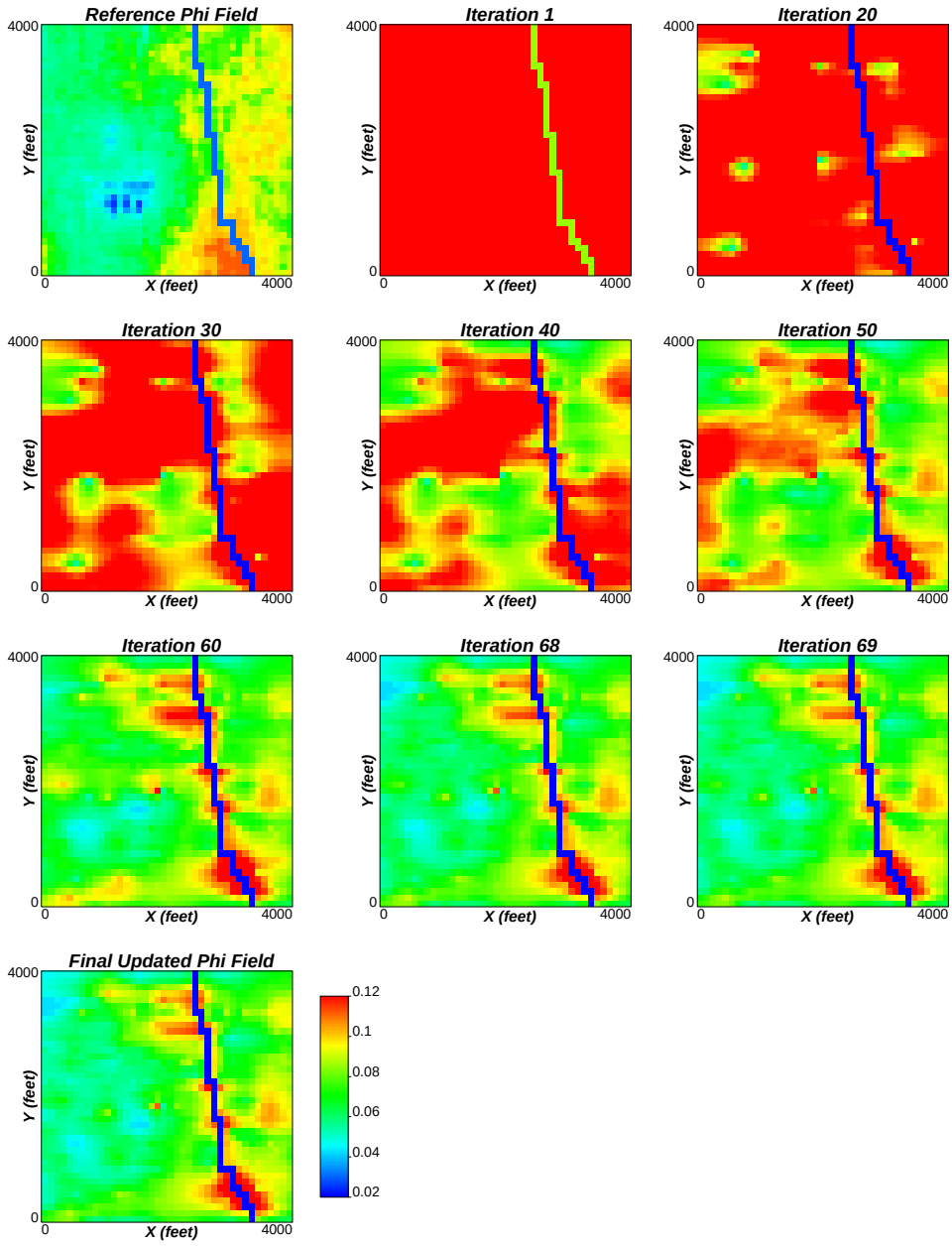

Figure 11: Updated ϕ fields at some iterations of the inversion process: Sealing Fault Example (Case A).

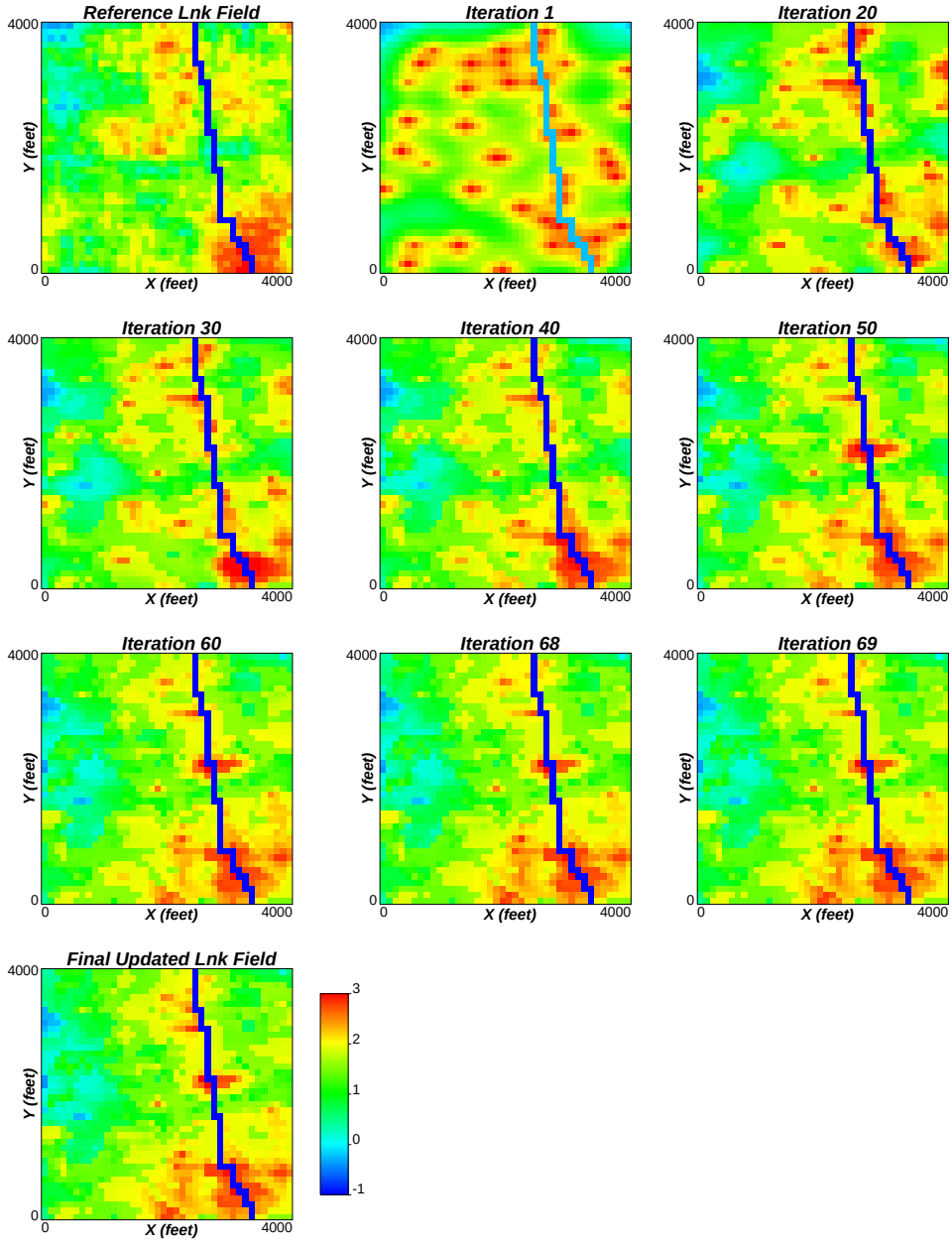

Figure 12: Updated $\ln(k)$ fields at some iterations of the inversion process: Sealing Fault Example (Case A).

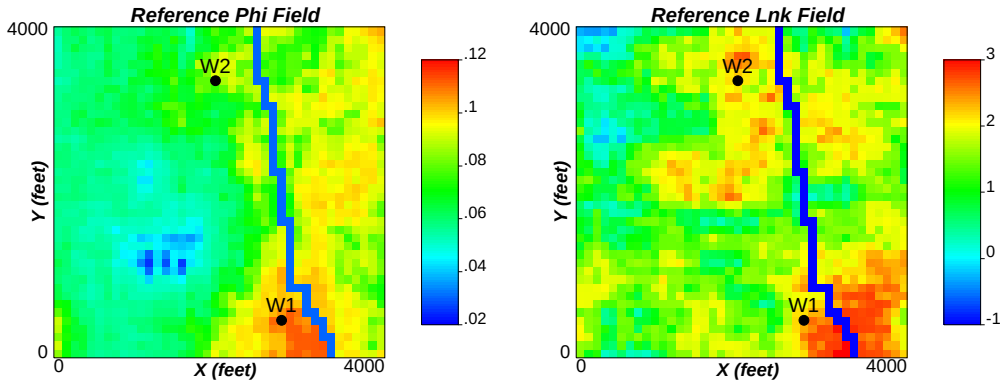

Figure 13: Reference faulted ϕ and $\ln(k)$ fields: Sealing Fault Example (Case B).

kept unchanged. Figure 14 shows the imposed production rates and the corresponding numerically simulated pressure responses at the two wells.

The inverted models are obtained after 216 outer iterations (59.5 minutes in a 1.8 GHz processor personal computer). The pressure responses in the updated porosity and permeability fields converge to the reference pressure data. These inverted models, shown in Figure 15, have a similar heterogeneity distribution to the reference truth. Figure 16 shows the pressure values at the two wells computed from the true (from reference), initial and final updated porosity and permeability fields. The objective function values of the inversion process is shown in Figure 17. Final average pressure mismatch (in L^2 norm sense) was 4.091 psi. The fault zone properties at all outer iterations are shown in Figures 18 and 19 for porosity and permeability values. Updated porosity and permeability fields after each outer iteration of the inversion method are shown in Figures 20 and 21.

Some Conclusions

Comparison of the two cases reveal that it is more likely that one can capture heterogeneity information from production data when the wells are in the opposite sides of the fault and there exists interference information in the production data. Inversion in Case B takes a significantly higher number of iterations to achieve the same order of pressure match and consequently higher CPU time than that in Case A. In fact, fault permeability values (see Figure 19) are much higher than the reference values. One can attribute the reason for poor resolution to the fact that there is less interference information available in the production data in Case B. Another observation is that fault permeability values are better resolved with the production data than the porosity values.

High Permeability Fault Example

In this section, we discuss the inversion of the properties of a high permeability fault. Similar two-well cases are analyzed in this exercise. All the information are kept unchanged as in the previous section unless stated otherwise.

Case A: 2 Wells on the Opposite Side of the Fault

The reference porosity and permeability fields are shown in Figure 22. Figure 23 shows the imposed production rates and the corresponding numerically simulated pressure responses at the two wells. The histogram and the scatter-plot between ϕ and $\ln(k)$ are shown in Figures 24 and 25, respectively. Mean and standard deviation of reference distributions are 0.073 and 0.018 for ϕ, and 1.661 and 1.131 for $\ln(k)$. The low average porosity confirms the low storativity of the reservoir. The correlation coefficient between porosity and permeability is 0.462. The fault location is the same as in the previous section. The reference fault zone porosity and $\ln(k)$ are 0.1 and 7.0.

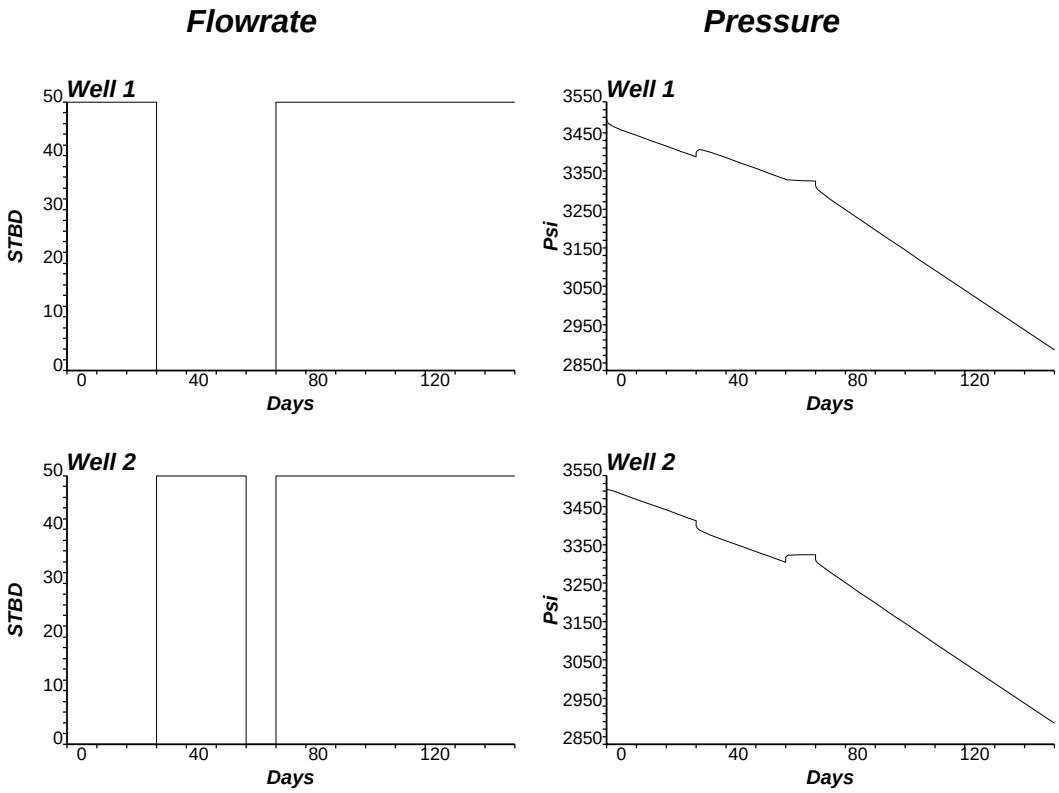

Figure 14: Production data (pressure and flow rates) obtained for 2 wells from the reference field: Sealing Fault Example (Case B).

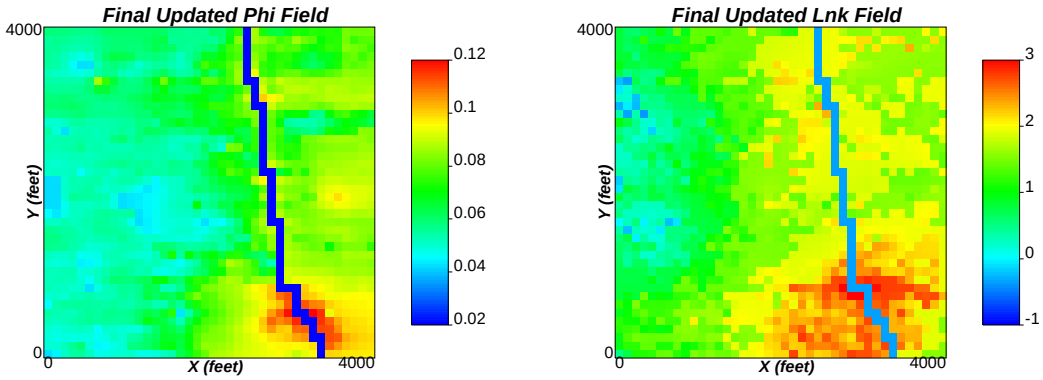

Figure 15: Updated ϕ and $\ln(k)$ fields: Sealing Fault Example (Case B).

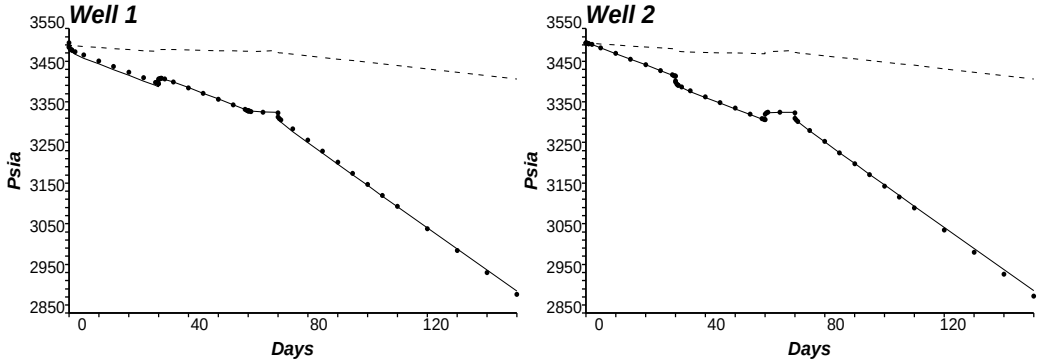

Figure 16: Pressure responses computed from initial (dashed lines) and updated (bullets) ϕ and $\ln(k)$ fields with the true data (solid lines): Sealing Fault Example (Case B).

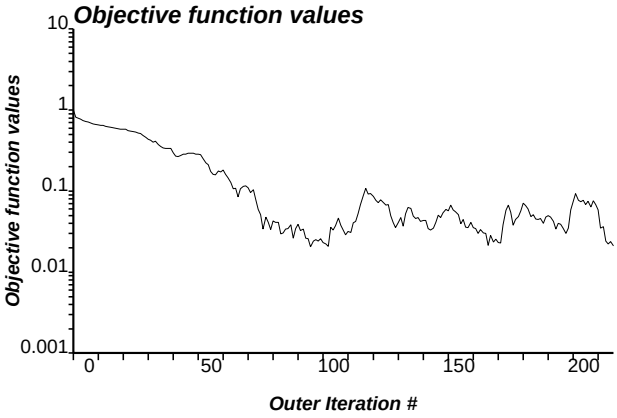

Figure 17: Objective function values of the inversion process: Sealing Fault Example (Case B).

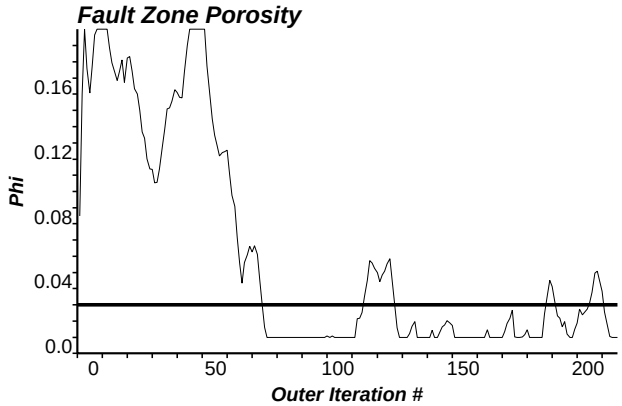

Figure 18: Fault zone ϕ values for each outer iteration: Sealing Fault Example (Case B). (Reference value: thicker horizontal line)

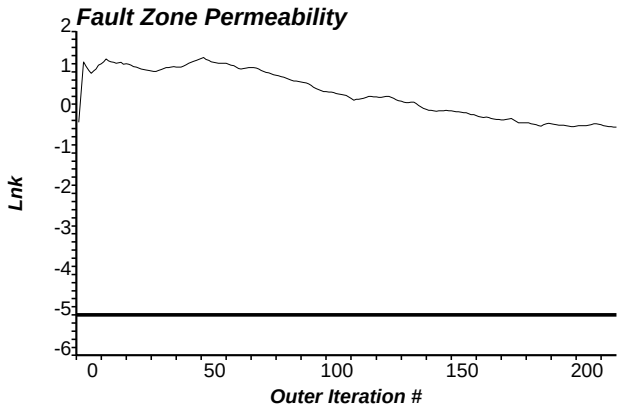

Figure 19: Fault zone $\ln(k)$ values for each outer iteration: Sealing Fault Example (Case B). (Reference value: thicker horizontal line)

The inverted models are obtained after 95 outer iterations (23.2 minutes in a 1.8 GHz processor personal computer). The pressure responses in the updated porosity and permeability fields converge to the reference pressure data. These inverted models are shown in Figure 26. Figure 27 shows the pressure values at the ten wells computed from the true (from reference), initial and final updated porosity and permeability fields. Final pressure match is remarkable. Final average pressure mismatch (in L^2 norm sense) was only 5.55 psi. The objective function values of the inversion process are shown in Figure 28. The fault zone properties at all outer iterations are shown in Figures 29 and 30 for porosity and permeability values. Updated porosity and permeability fields at some outer iterations of the inversion method are shown in Figures 31 and 32.

Case B: 2 Wells in the Same Side of the Fault

The wells are shown in Figure 33. Figure 34 shows the imposed production rates and the corresponding numerically simulated pressure responses at the two wells. The inverted models are obtained after 100 outer iterations (25.2 minutes in a 1.8 GHz processor personal computer). The pressure responses in the updated porosity and permeability fields converge to the reference pressure data. These inverted models, shown in Figure 35, have a similar heterogeneity distribution to the reference truth. Figure 36 shows the pressure values at the two wells computed from the true (from reference), initial and final updated porosity and permeability fields. The objective function values of the inversion process is shown in Figure 37. Final average pressure mismatch (in L^2 norm sense) was 3.002 psi. The fault zone properties at all outer iterations are shown in Figures 38 and 39 for porosity and permeability values. Updated porosity and permeability fields after each outer iteration of the inversion method are shown in Figures 40 and 41.

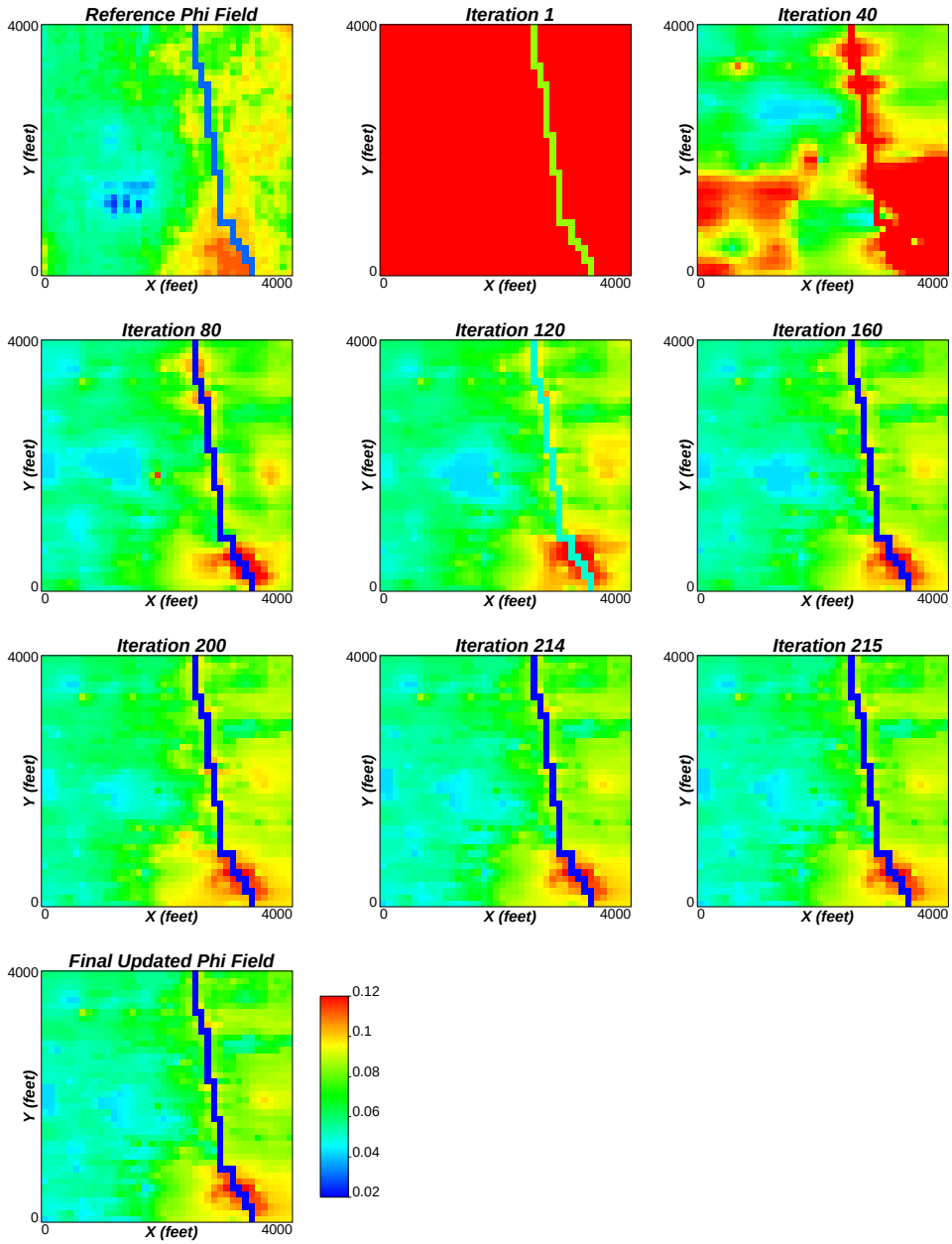

Figure 20: Updated ϕ fields at some iterations of the inversion process: Sealing Fault Example (Case B).

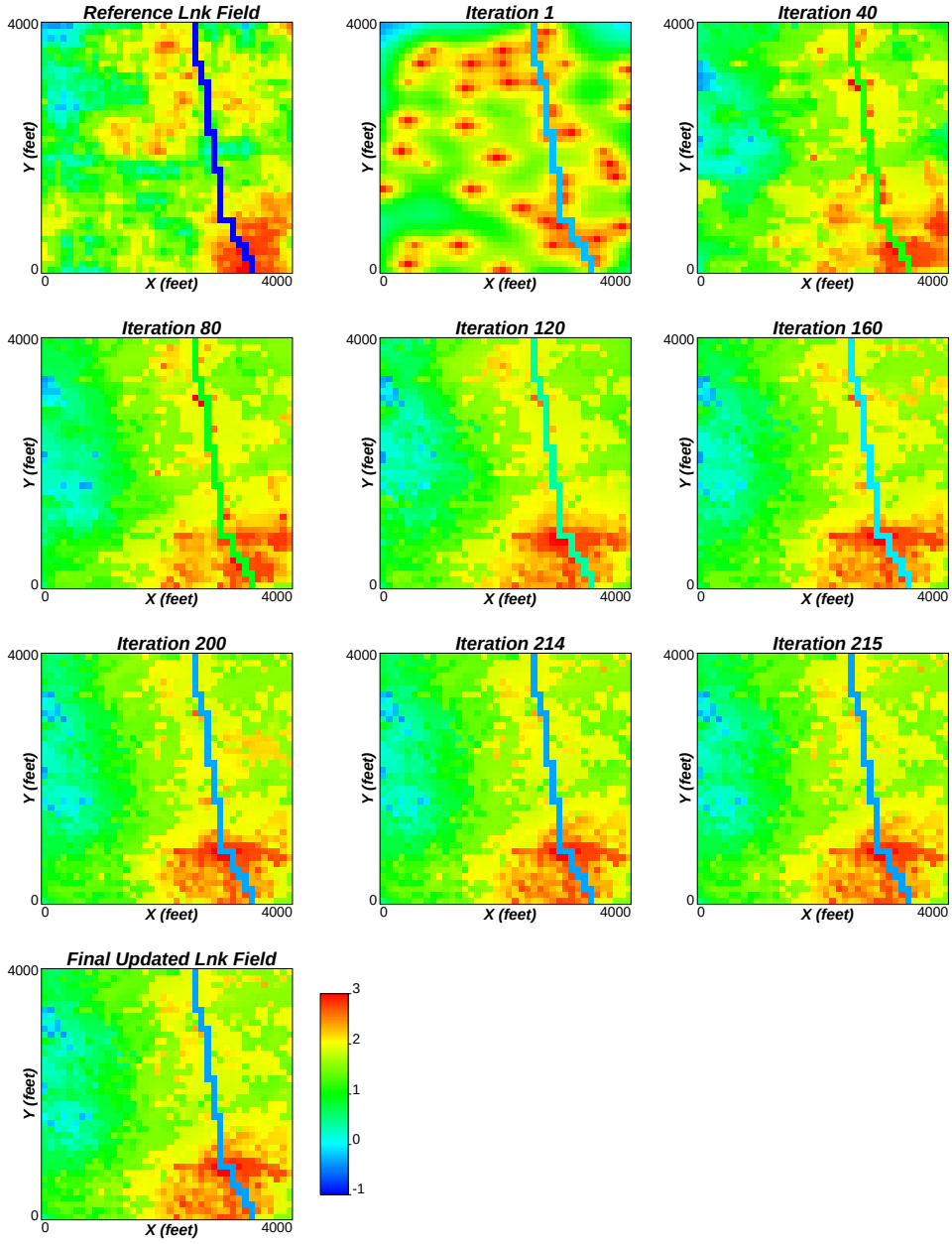

Figure 21: Updated $\ln(k)$ fields at some iterations of the inversion process: Sealing Fault Example (Case B).

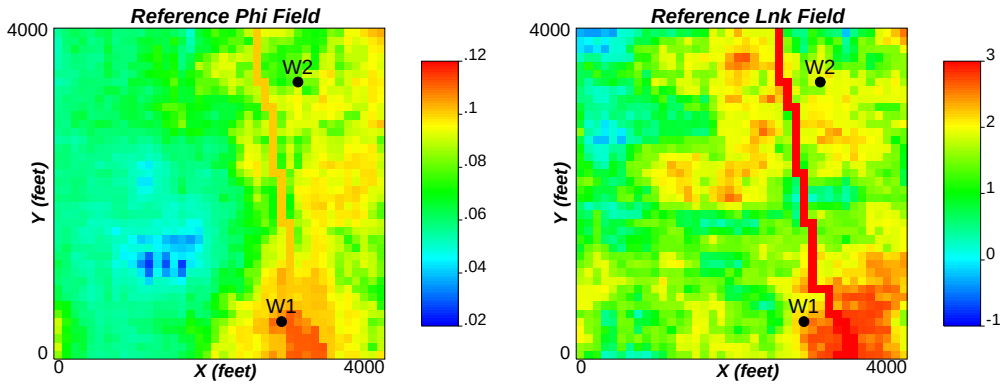

Figure 22: Reference faulted ϕ and $\ln(k)$ fields: High Permeability Fault Example (Case A).

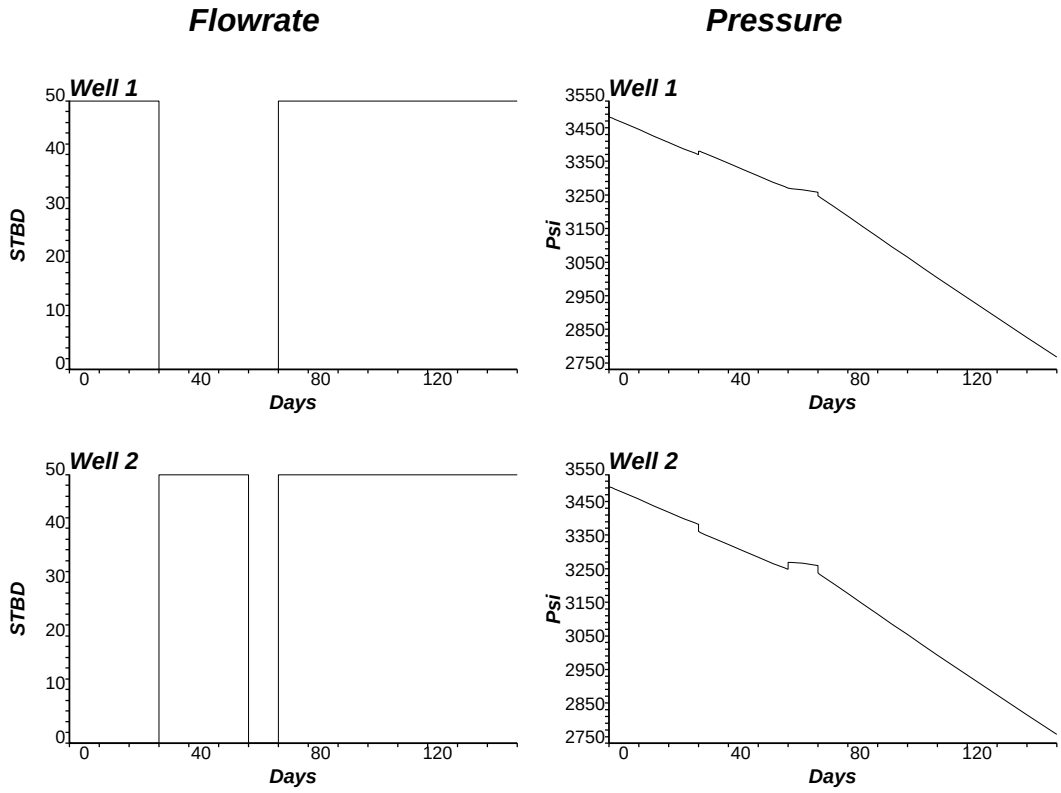

Figure 23: Production data (pressure and flow rates) obtained for 2 wells from the reference field: High Permeability Fault Example (Case A).

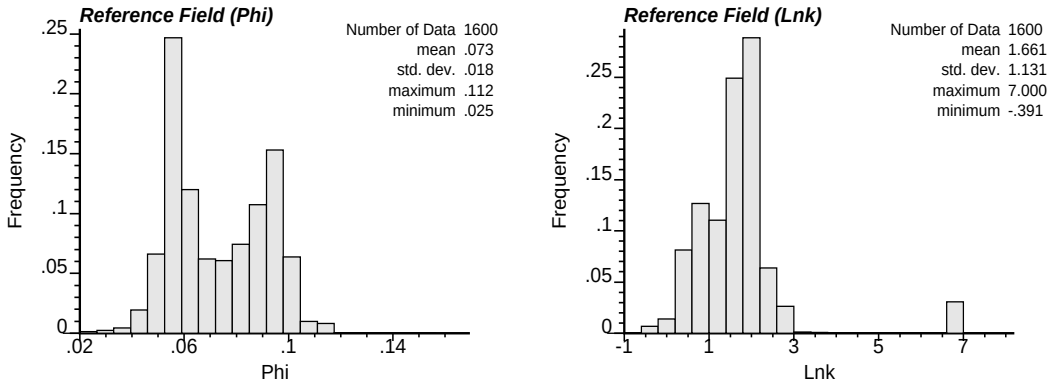

Figure 24: Histograms of reference ϕ and $\ln(k)$ fields: High Permeability Fault Example (Case A).

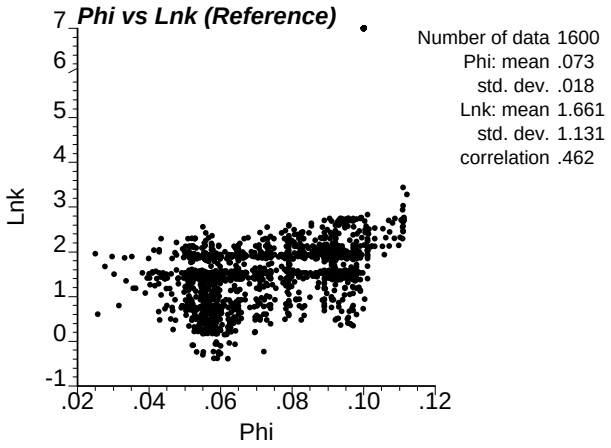

Figure 25: Scatterplot of reference ϕ and $\ln(k)$ distributions: High Permeability Fault Example (Case A).

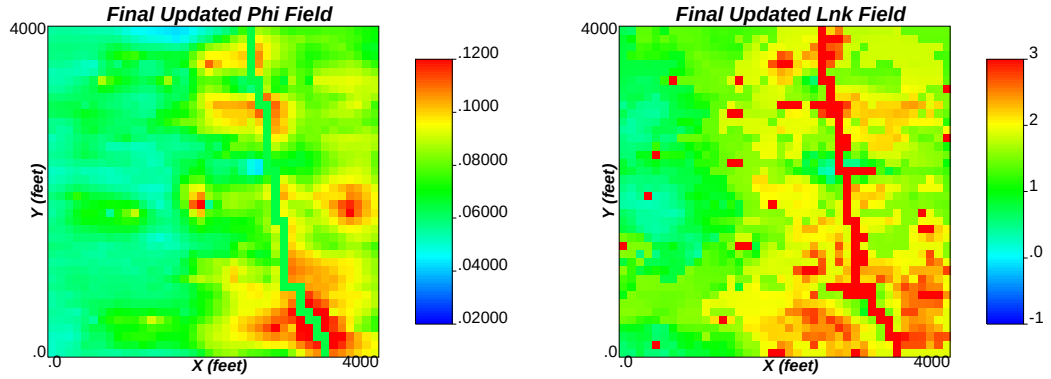

Figure 26: Updated ϕ and $\ln(k)$ fields: High Permeability Fault Example (Case A).

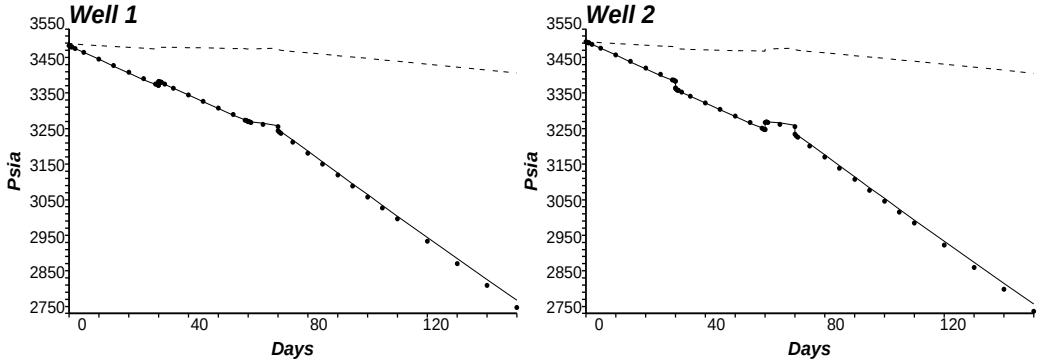

Figure 27: Pressure responses computed from initial (dashed lines) and updated (bullets) ϕ and $\ln(k)$ fields with the true data (solid lines): High Permeability Fault Example (Case A).

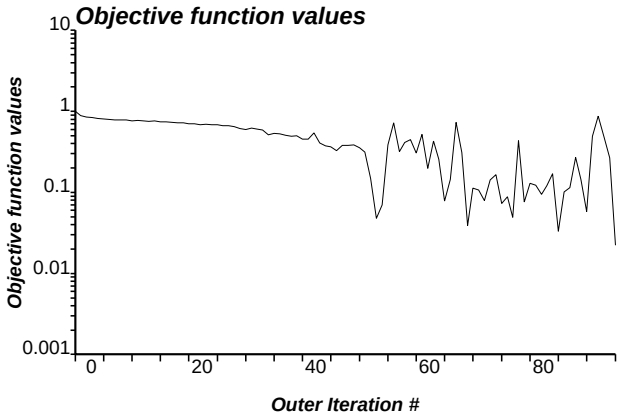

Figure 28: Objective function values of the inversion process: High Permeability Fault Example (Case A).

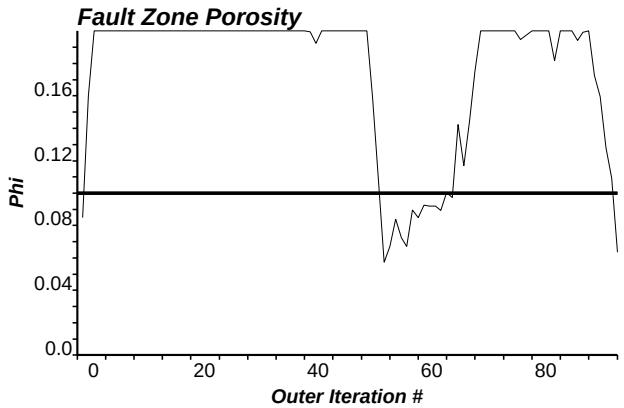

Figure 29: Fault zone ϕ values at each outer iteration: High Permeability Fault Example (Case A). (Reference value: thicker horizontal line)

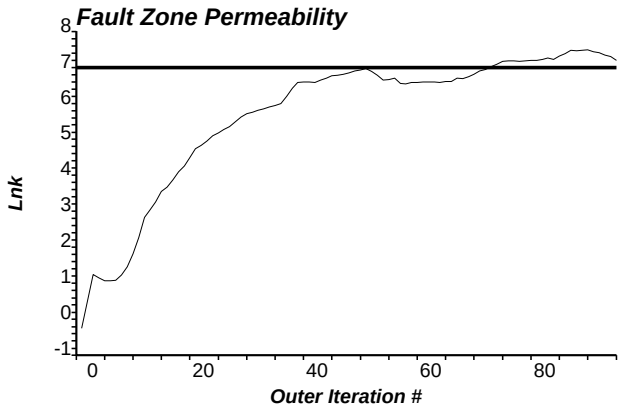

Figure 30: Fault zone ln(k) values at each outer iteration: High Permeability Fault Example (Case A). (Reference value: thicker horizontal line)

Some Conclusions

For the high permeability fault, the inversion outcomes with both the cases changing the well locations show that reservoir heterogeneity is not captured well as in the situation with sealing faults. However, the objective values do converge faster in this case. Analyzing the objective function values (Figures 28 and 37), it is evident that jump in the values are drastic in this case. The reason for such jumps may be attributed to the erratic nature of the fault porosity values. There is clearly no convergence in the fault porosity values (Figures 29 and 38).

The other observation is that both the well location cases show similar nature of inverted outcomes. It is intuitively expected because with high permeability fault the well locations will not matter much. The wells will almost be in instantaneous communication with each other.

Sensitivity Studies

Sensitivity of the inversion solution to certain parameters in the inversion process was investigated. The sensitivity to prior fault zone ln(k) values and the number of fault zone master points are discussed below. Some general inversion related sensitivity studies were performed in [1].

Sensitivity to Prior Information

For the inversion of the fault properties, the code requires inputs of a priori fault zone ln(k) and ϕ, which may affect on the inversion solution. For the base case, we have the result of sealing fault example Case A (that is, the wells are in the opposite side of the fault). For the base case, we used a priori fault zone ln(k) of -1.0 and ϕ of 0.01. In this sensitivity study, we employed in one run ln(k) value of 1.0 and ϕ of 0.01, while in another run these values were 1.0 and 0.1. Figures 42 and 43 show the updated porosity and permeability fields. These figures should be compared with Figure 6. Inverted fault zone ln(k) and ϕ values at each outer iteration of the inversion process are shown in Figures 45 and 46 for the three cases. The number of outer iterations for the convergence were 166, 124 and 70 for the three cases. Objective function values at each outer iteration are shown in Figure 44 for the cases. Corresponding final objective function L^2 norm values are 2.573, 2.843 and 2.527, respectively. It should be mentioned that the fault zone ln(k) and ϕ in the reference field are -5.0 and 0.03. Analyzing Figures 45 and 46 and the final objective function values that the inversion outcomes are more or less robust to prior information.

Sensitivity to Number of Fault Zone Master Points

We performed a sensitivity study to number of fault zone master points. Most of the results shown in this work are done with 8 master points for the fault zone. We analyze the inversion solution

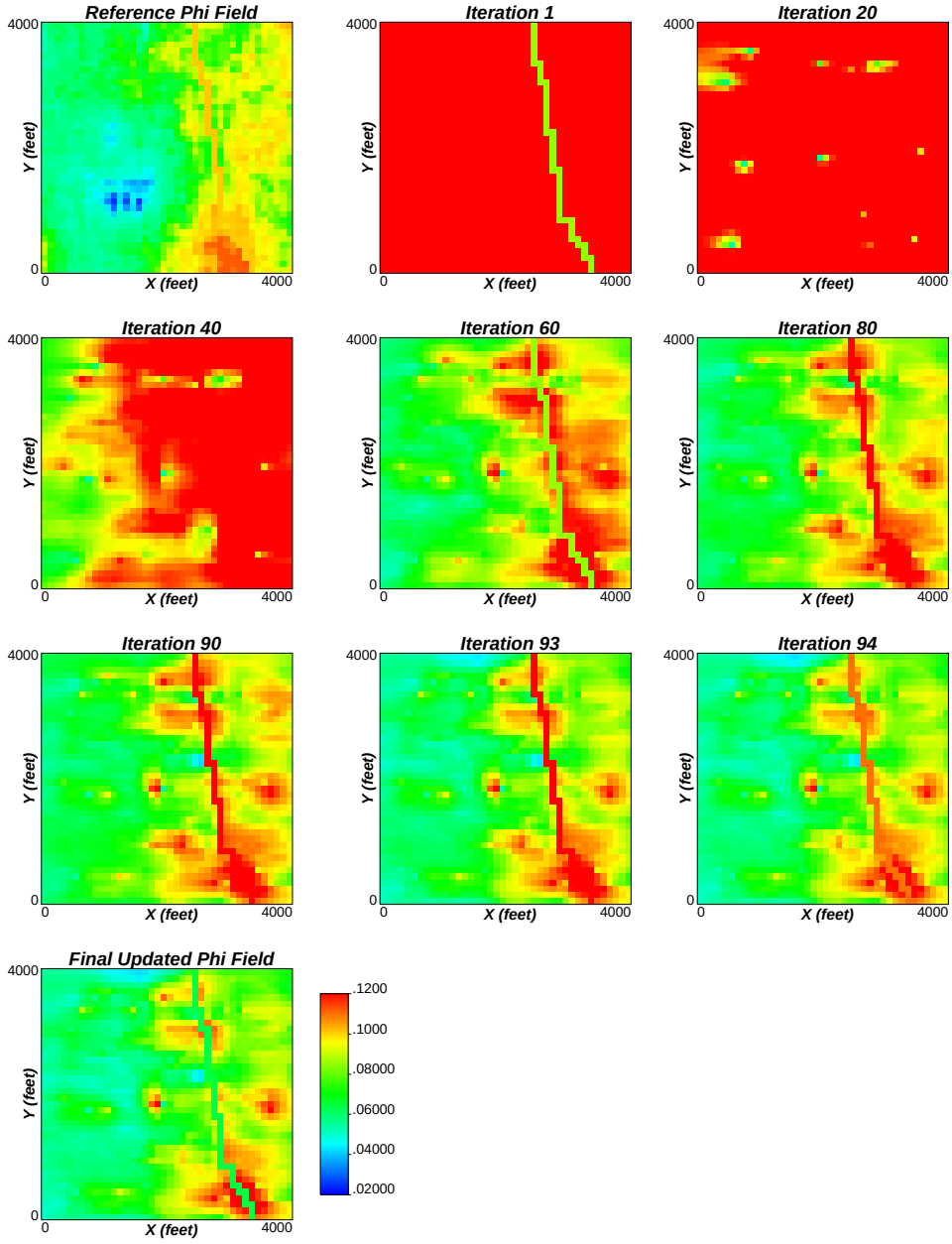

Figure 31: Updated ϕ fields at some iterations of the inversion process: High Permeability Fault Example (Case A).

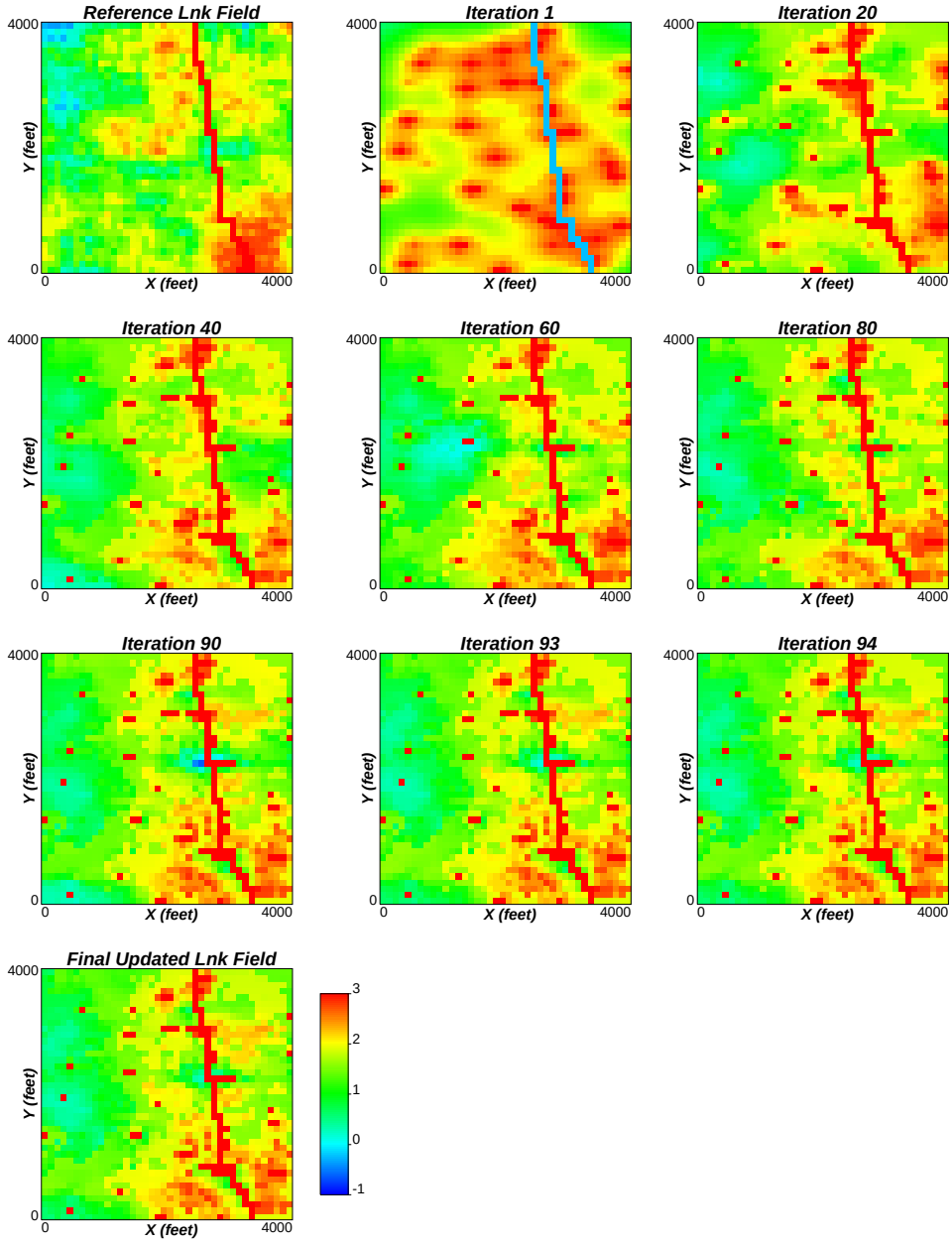

Figure 32: Updated $\ln(k)$ fields at some iterations of the inversion process: High Permeability Fault Example (Case A).

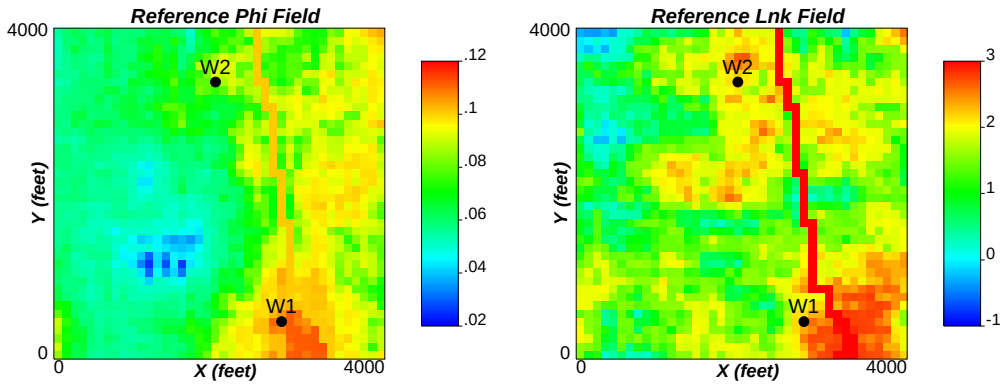

Figure 33: Reference faulted ϕ and $\ln(k)$ fields: High Permeability Fault Example (Case B).

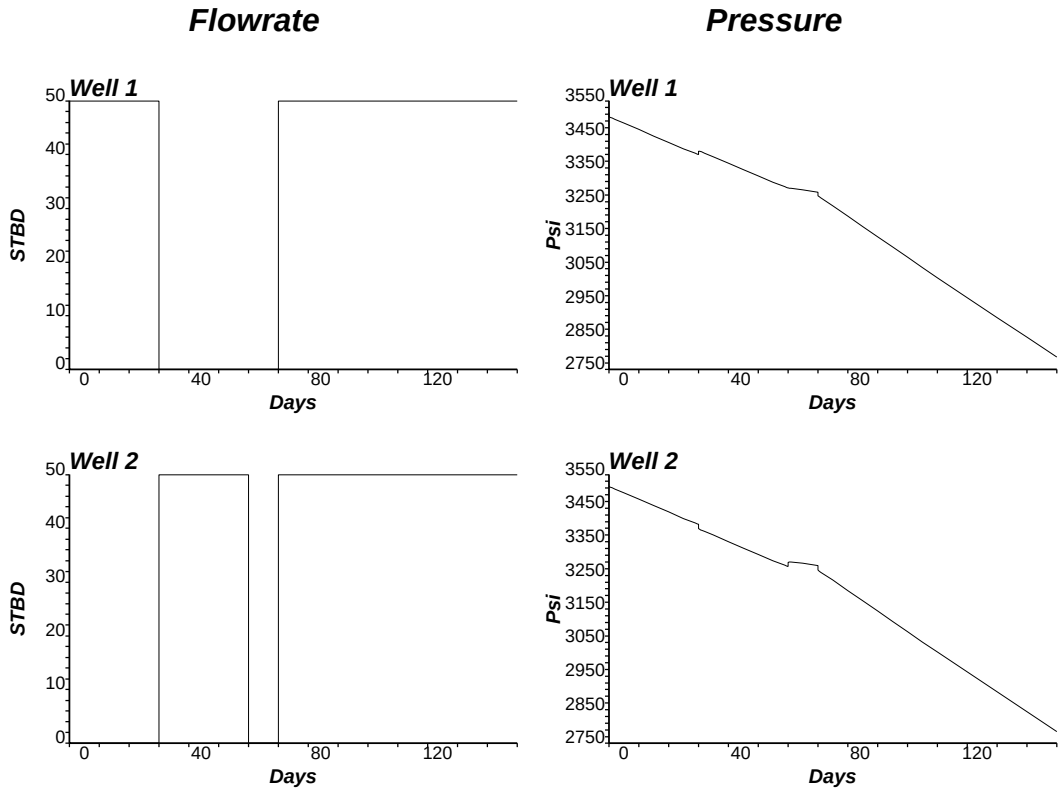

Figure 34: Production data (pressure and flow rates) obtained for 2 wells from the reference field: High Permeability Fault Example (Case B).

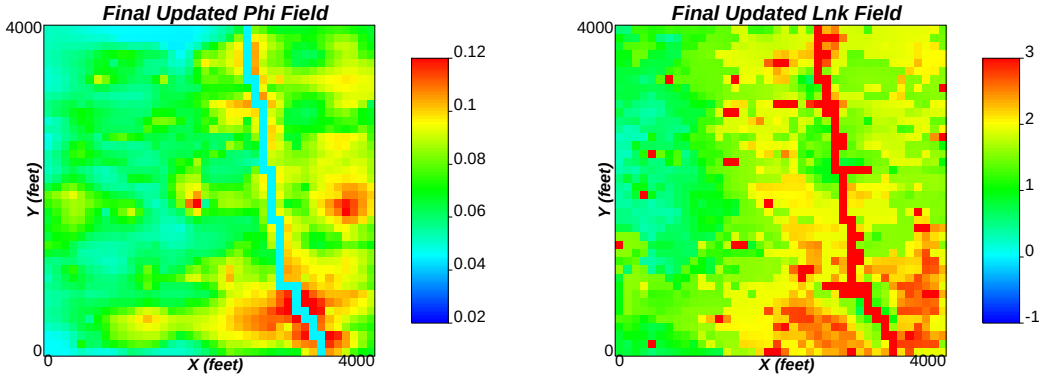

Figure 35: Updated ϕ and $\ln(k)$ fields: High Permeability Fault Example (Case B).

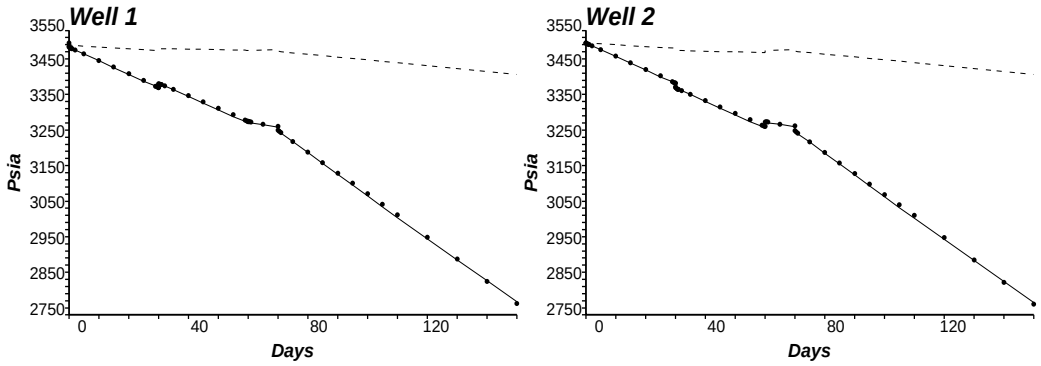

Figure 36: Pressure responses computed from initial (dashed lines) and updated (bullets) ϕ and $\ln(k)$ fields with the true data (solid lines): High Permeability Fault Example (Case B).

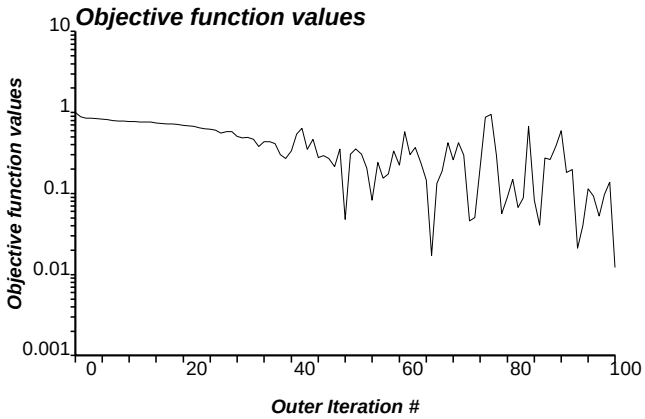

Figure 37: Objective function values of the inversion process: High Permeability Fault Example (Case B).

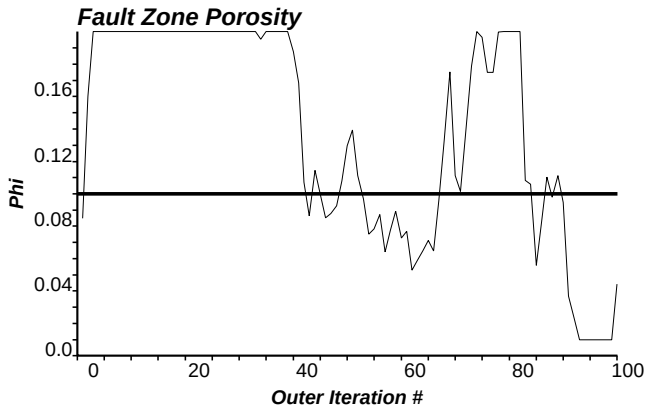

Figure 38: Fault zone ϕ values for each outer iteration: High Permeability Fault Example (Case B). (Reference value: thicker horizontal line)

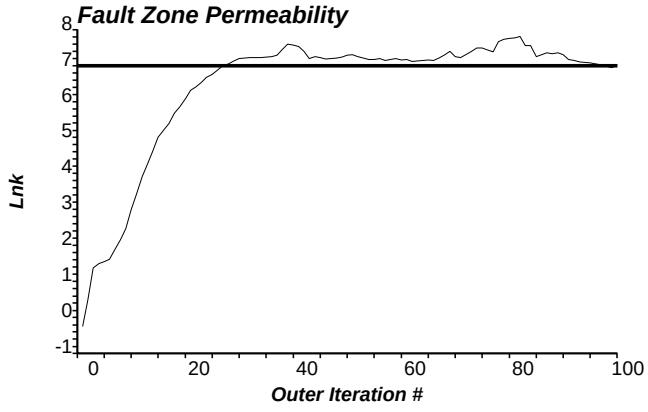

Figure 39: Fault zone $\ln(k)$ values for each outer iteration: High Permeability Fault Example (Case B). (Reference value: thicker horizontal line)

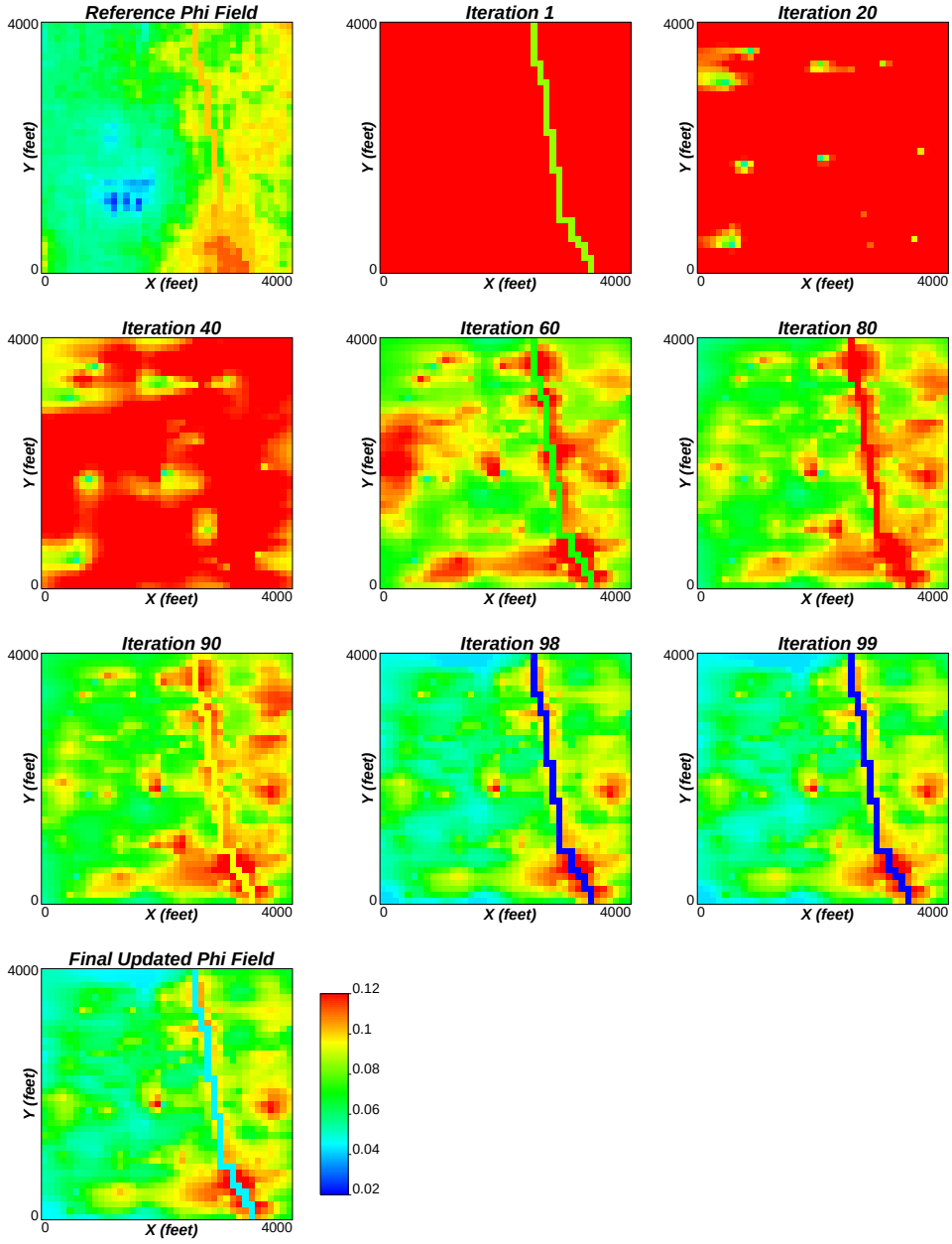

Figure 40: Updated ϕ fields at some iterations of the inversion process: High Permeability Fault Example (Case B).

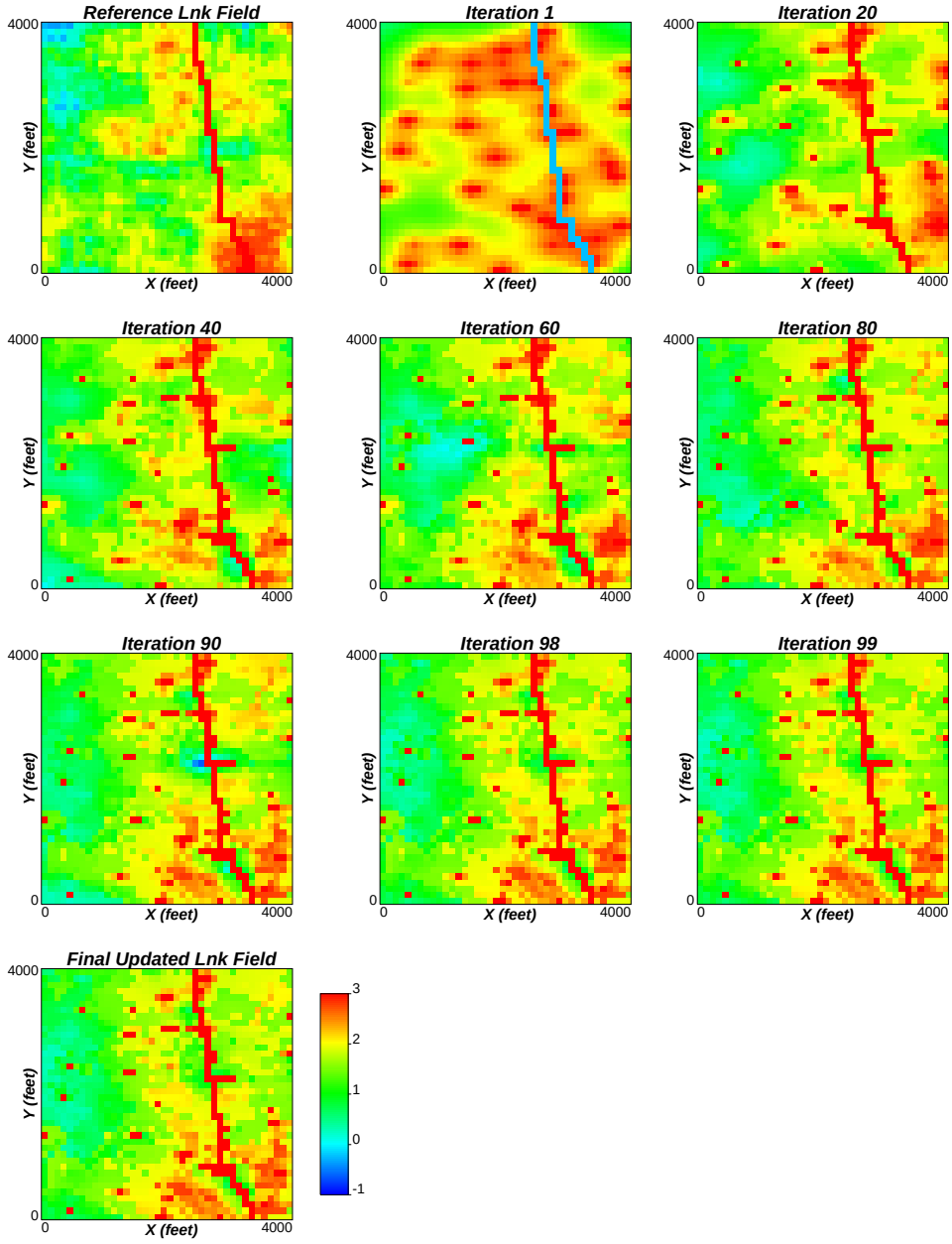

Figure 41: Updated $\ln(k)$ fields at some iterations of the inversion process: High Permeability Fault Example (Case B).

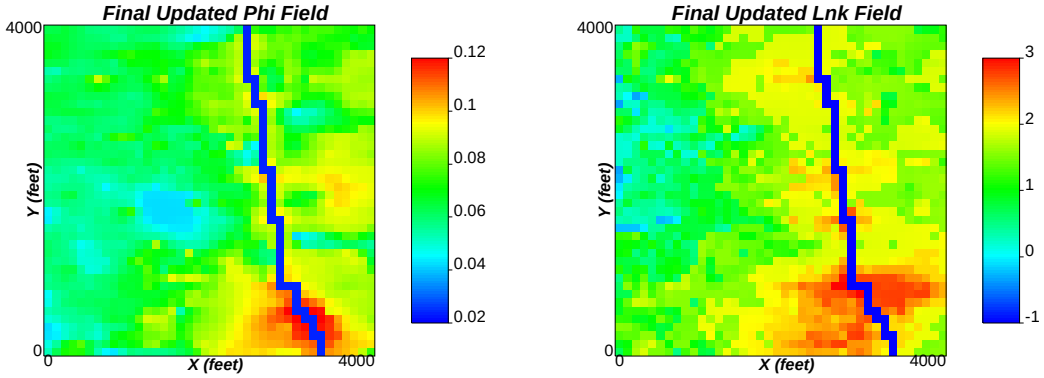

Figure 42: Updated ϕ and $\ln(k)$ fields: A Priori Fault Zone $\ln(k)$ of 1.0 and ϕ of 0.01.

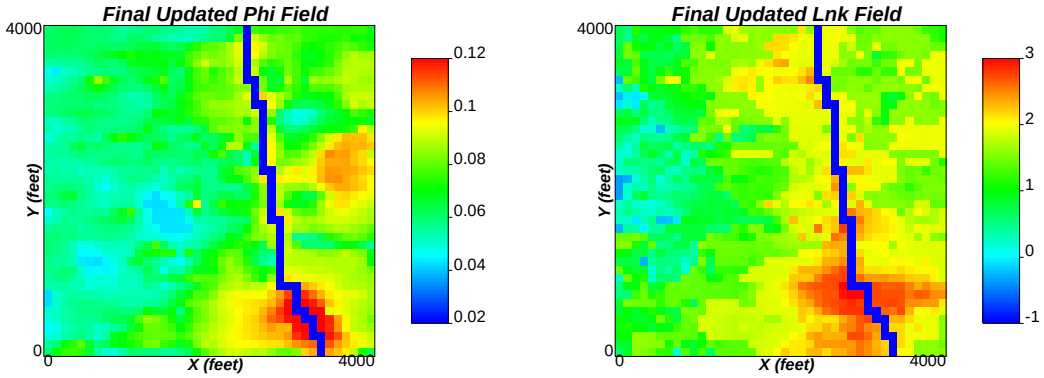

Figure 43: Updated ϕ and $\ln(k)$ fields: A Priori Fault Zone $\ln(k)$ of 1.0 and ϕ of 0.1.

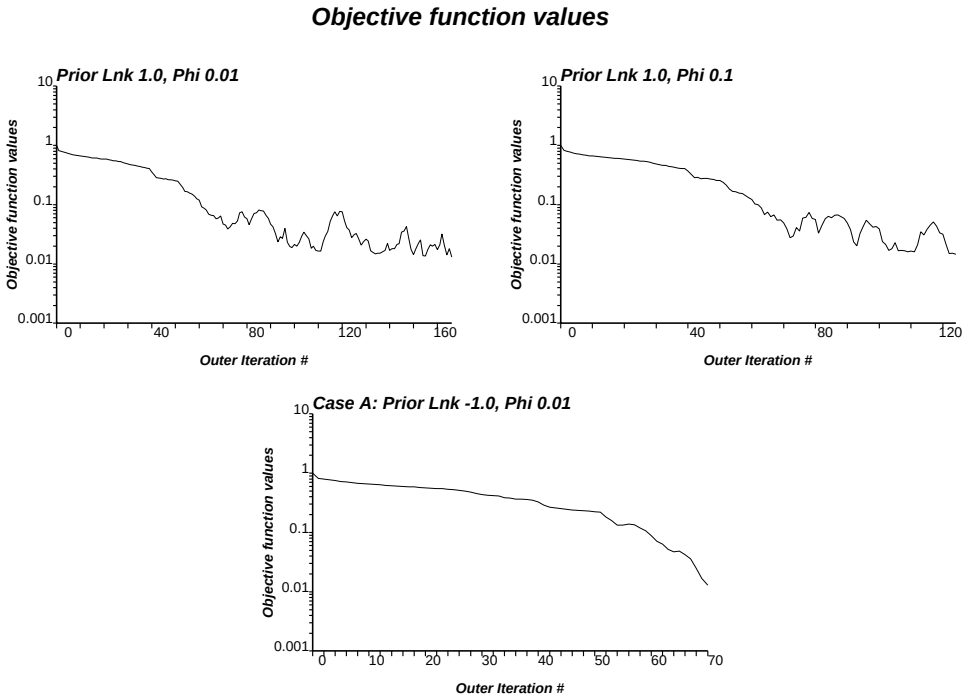

Figure 44: Objective function values at each outer iteration for different a priori values.

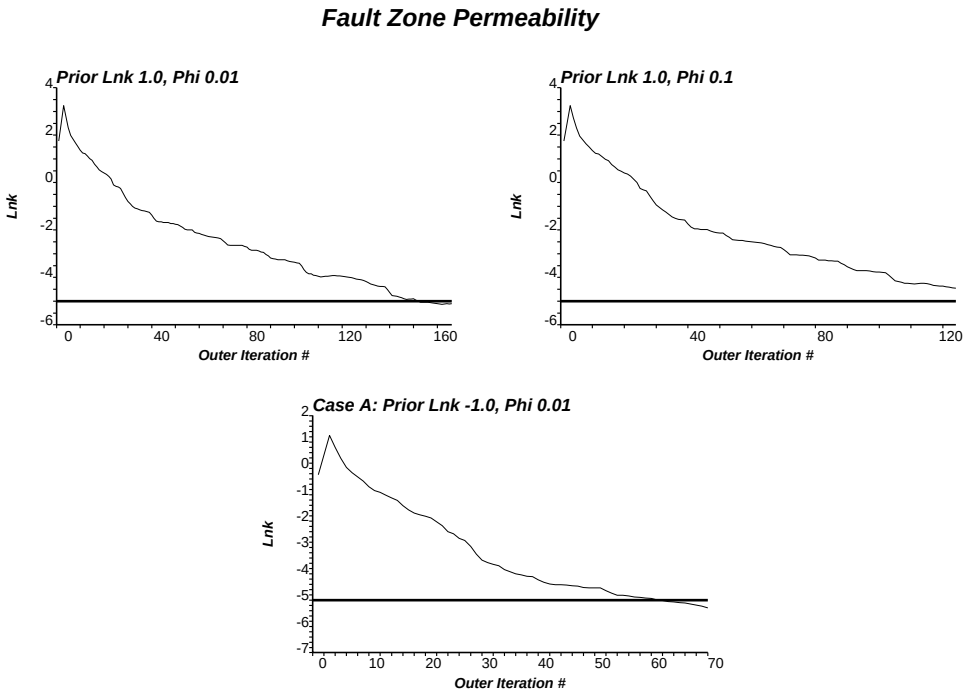

Figure 45: Fault zone $\ln(k)$ values at each outer iteration for different a priori values. (Reference value: thicker horizontal line)

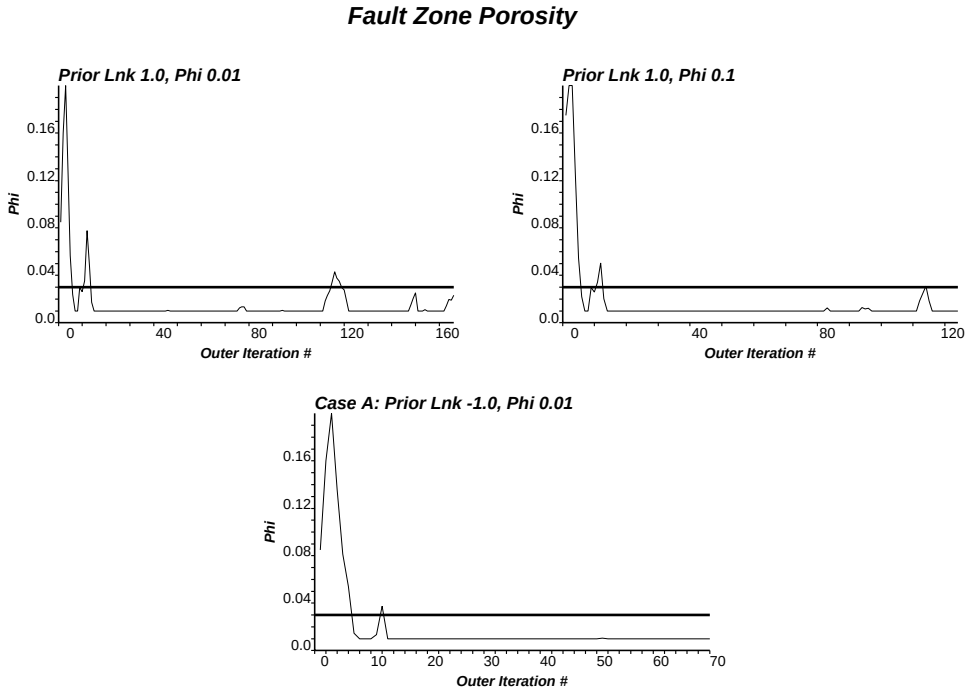

Figure 46: Fault zone ϕ values at each outer iteration for different a priori values. (Reference value: thicker horizontal line)

with 6, 8 and 10 fault zone master points. For this sensitivity exercise, we again use the sealing fault exercise Case A (where we used 8 master points) as the base case.

Figures 47 and 48 show the updated porosity and permeability fields for the two cases with 6 and 10 master points. Inverted fault zone $\ln(k)$ values at each outer iteration of the inversion process are shown in Figure 50 for the three cases. Corresponding inverted fault zone ϕ values are shown in Figure 51. It is evident from this figure that fault zone porosity inversion is not very robust. The number of outer iterations for the convergence were 102, 128 and 70 for the three cases. Objective function values at each outer iteration are shown in Figure 49 for the cases. Corresponding final objective function L^2 norm values are 2.598, 2.087 and 2.527, respectively. It should be mentioned that the fault zone $\ln(k)$ and ϕ in the reference field are -5.0 and 0.03. Analyzing Figures 50 and 51 and the final objective function values that the inversion outcomes are more or less robust to number of master points.

Effect of Production Data

In this section, we investigate how production data affects the inversion of fault properties. We perform the inversion with production data from 3 and 4 wells. We employ similar parameters as in the sealing fault (Case A) exercise apart from the production data. The well locations for both the cases are shown in Figure 52.

3 Well Case

The 3 wells are: W1 at the center of the cell (28, 5), W2 at (30, 34), and W3 at (20, 34). Figure 53 shows the imposed production rates and the corresponding numerically simulated pressure responses at these wells. The inversion was run for 293 outer iterations. CPU time for the run was only 80.1 minutes in a 1.8 GHz Pentium 4 machine. The pressure responses in the updated porosity and permeability fields converge to the reference pressure data. These inverted models are shown in Figure 54. Figure 55 shows the pressure values at the three wells computed from the true (from reference), initial and final updated porosity and permeability fields. The objective function values

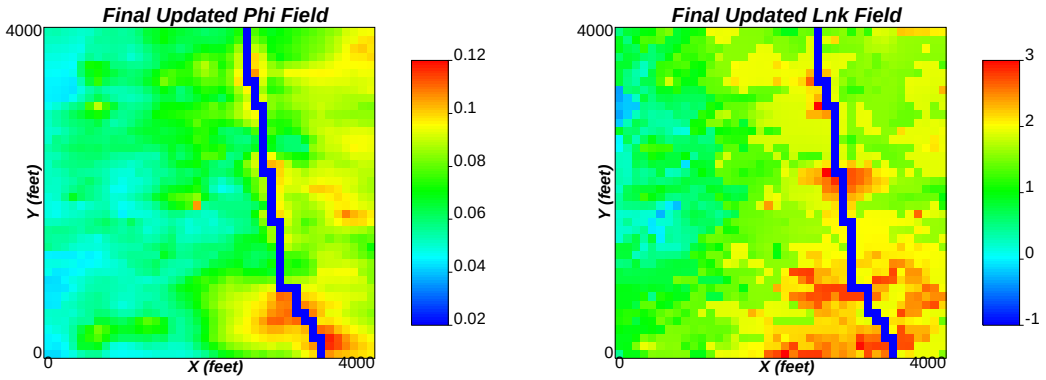

Figure 47: Updated ϕ and $\ln(k)$ fields honoring production data, local hard data, global distribution, prior variography information and prior fault zone $\ln(k)$ of -1.0 with 6 Master Point Case.

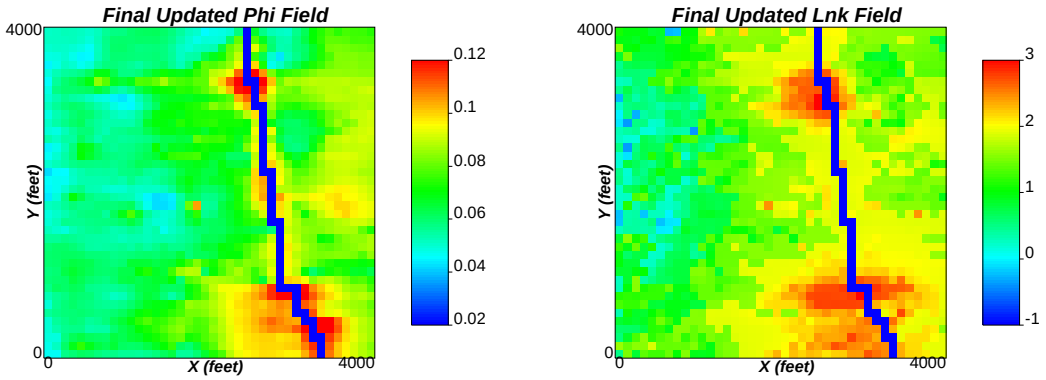

Figure 48: Updated ϕ and $\ln(k)$ fields: 10 Master Point Case.

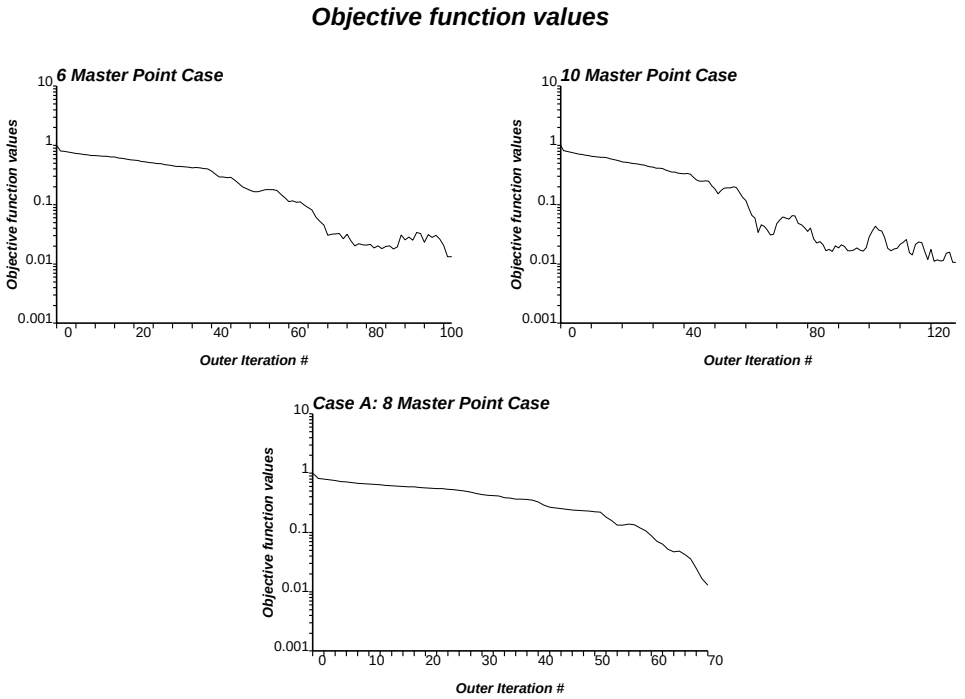

Figure 49: Objective function values at each outer iteration for varying number of master points.

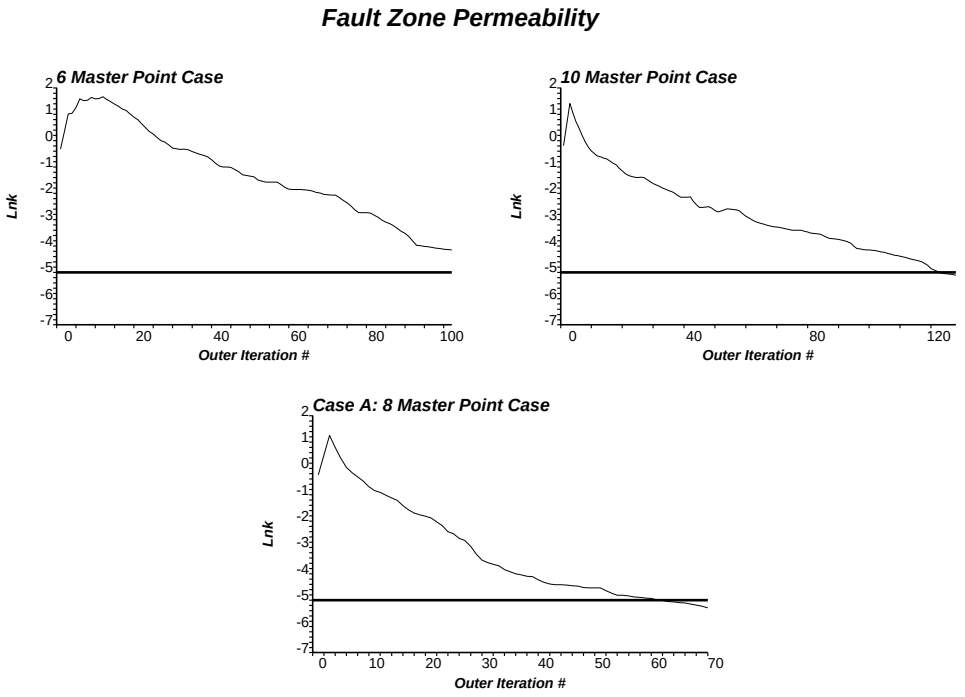

Figure 50: Fault zone $\ln(k)$ values at each outer iteration for varying number of master points. (Reference value: thicker horizontal line)

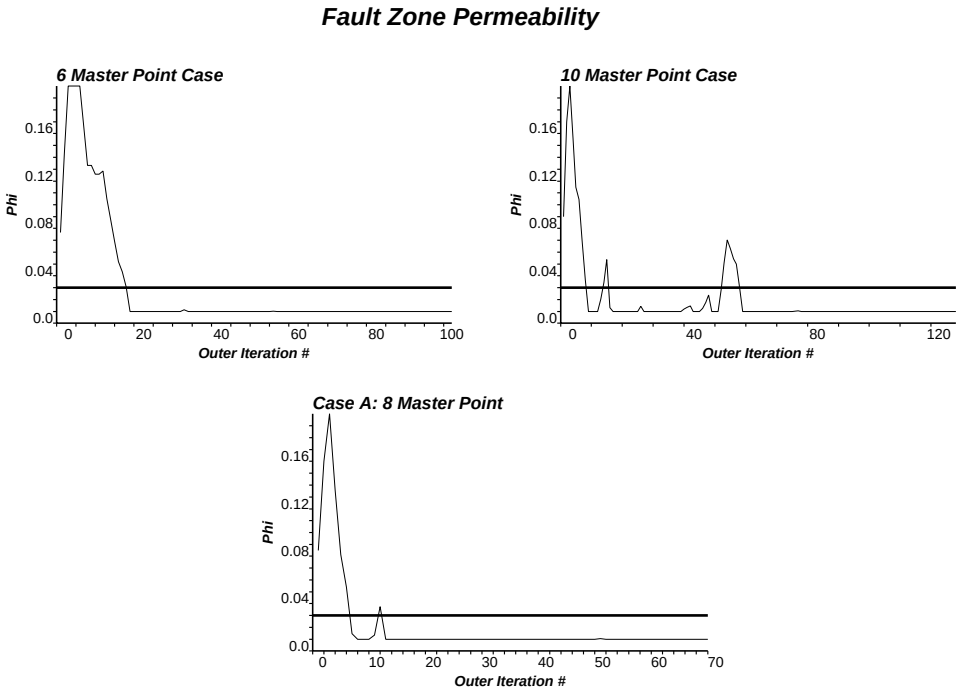

Figure 51: Fault zone ϕ values at each outer iteration for varying number of master points. (Reference value: thicker horizontal line)

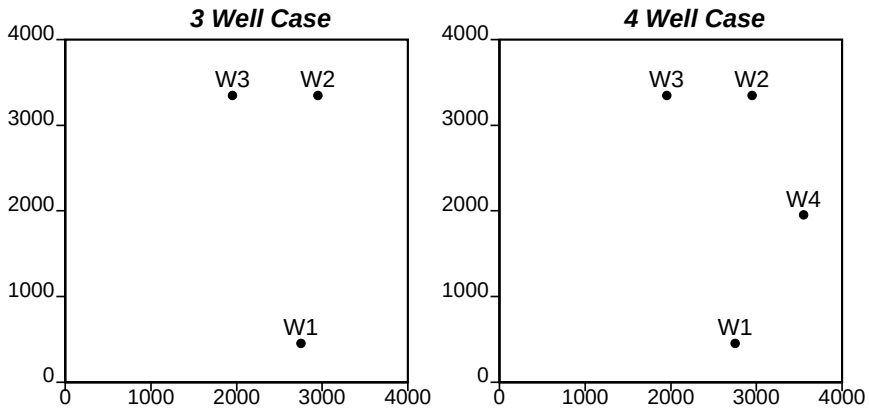

Figure 52: Well locations for 3 and 4 well cases.

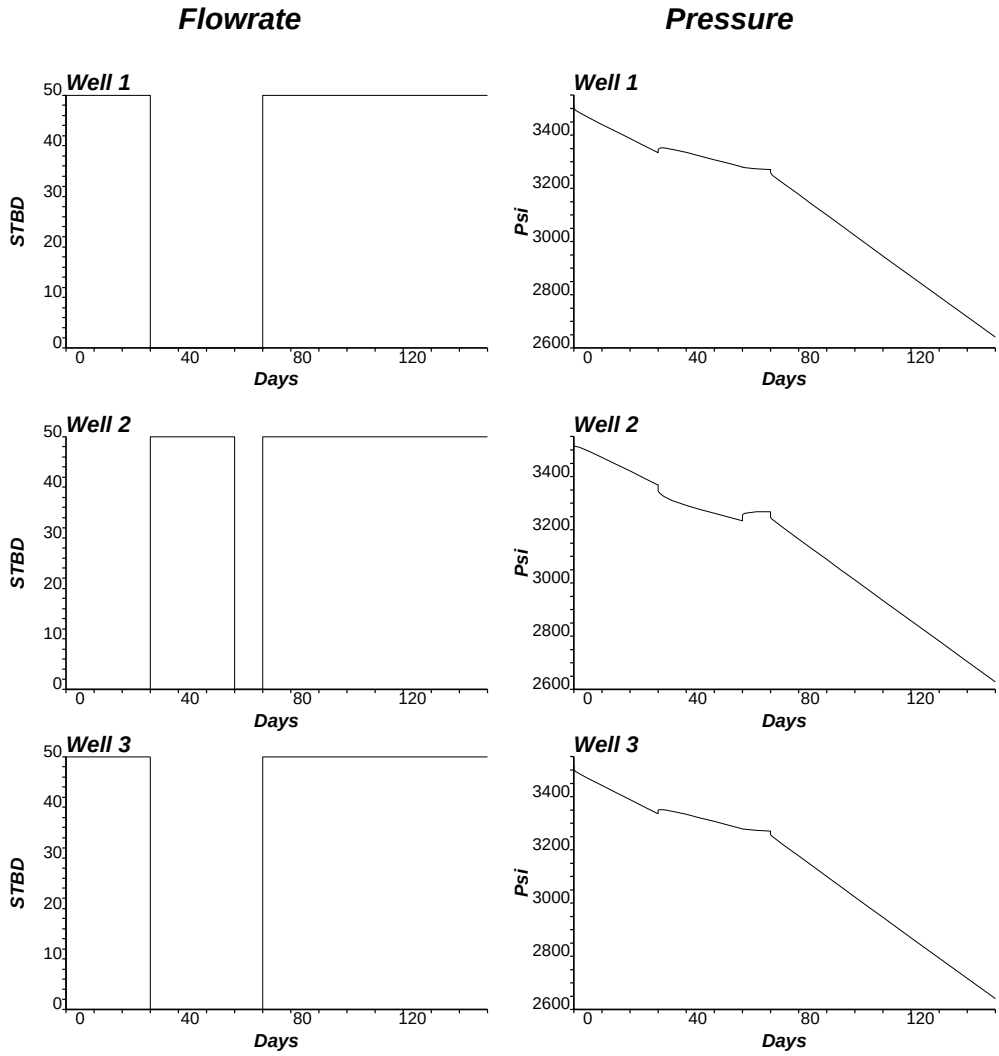

Figure 53: Production data (pressure and flow rates) obtained from the reference field: 3 Well Case.

of the inversion process is shown in Figure 56. Final average pressure mismatch in L^2 norm sense was 2.054 psi. The fault zone properties at all outer iterations are shown in Figures 57 and 58 for porosity and permeability values. Updated porosity and permeability fields at some outer iterations of the inversion method are shown in Figures 59 and 60.

4 Well Case

The 4 wells are: W1 at the center of the cell (28, 5), W2 at (30, 34), W3 at (20, 34), and W4 at (36, 20). Figure 61 shows the imposed production rates and the corresponding numerically simulated pressure responses at these wells. The inversion was run for 226 outer iterations. CPU time for the run was only 62.5 minutes in a 1.8 GHz Pentium 4 machine. The pressure responses in the updated porosity and permeability fields converge to the reference pressure data. These inverted models are shown in Figure 62. Figure 63 shows the pressure values at the four wells computed from the true (from reference), initial and final updated porosity and permeability fields. The objective function values of the inversion process is shown in Figure 64. Final average pressure mismatch in L^2 norm sense was 3.217 psi. The fault zone properties at all outer iterations are shown in Figures 65 and 66 for porosity and permeability values. Updated porosity and permeability fields at some outer iterations of the inversion method are shown in Figures 67 and 68.

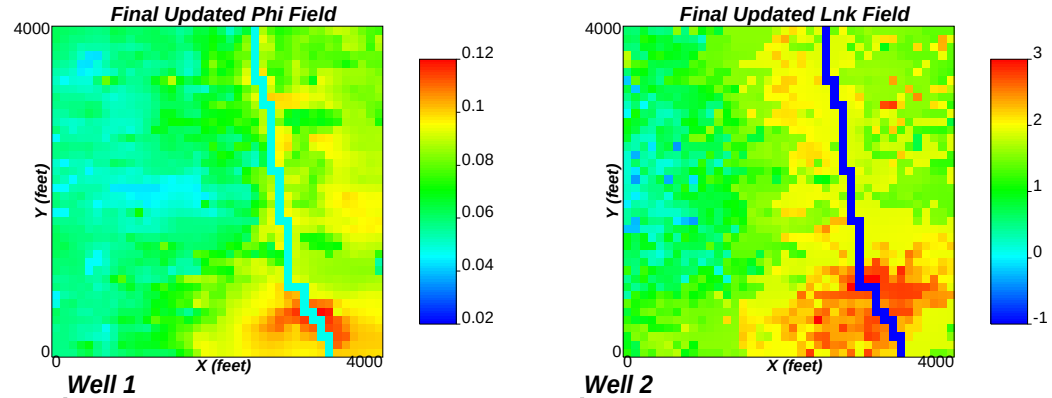

Figure 54: Updated ϕ and $\ln(k)$ fields: 3 Well Case.

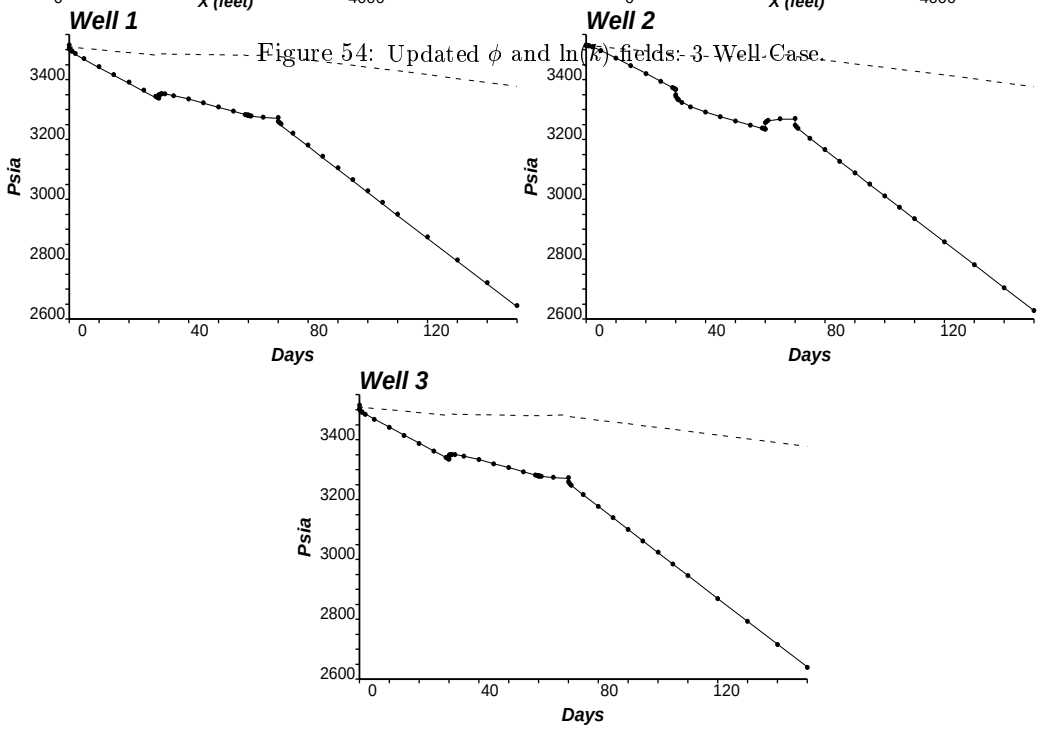

Figure 55: Pressure responses computed from initial (dashed lines) and updated (bullets) ϕ and $\ln(k)$ fields with the true data (solid lines): 3 Well Case.

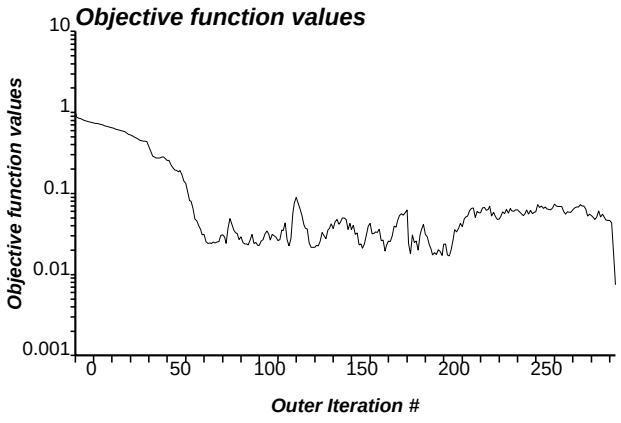

Figure 56: Objective function values of the inversion process: 3 Well Case.

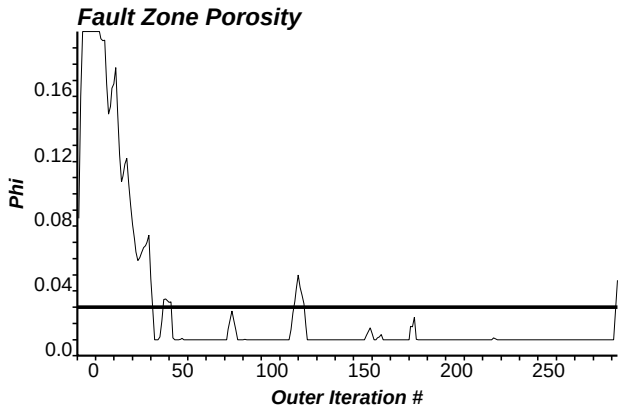

Figure 57: Fault zone ϕ values for each outer iteration: 3 Well Case. (Reference value: thicker horizontal line)

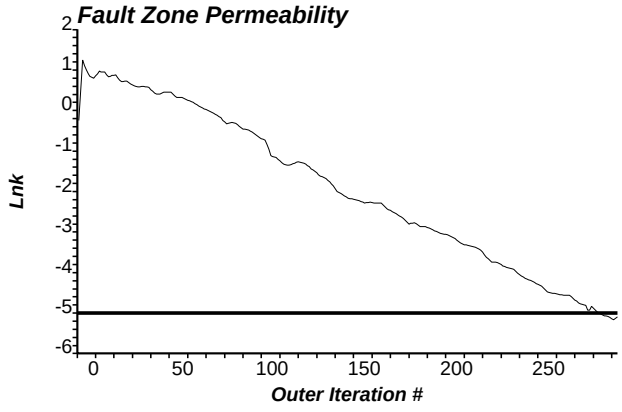

Figure 58: Fault zone $\ln(k)$ values for each outer iteration: 3 Well Case. (Reference value: thicker horizontal line)

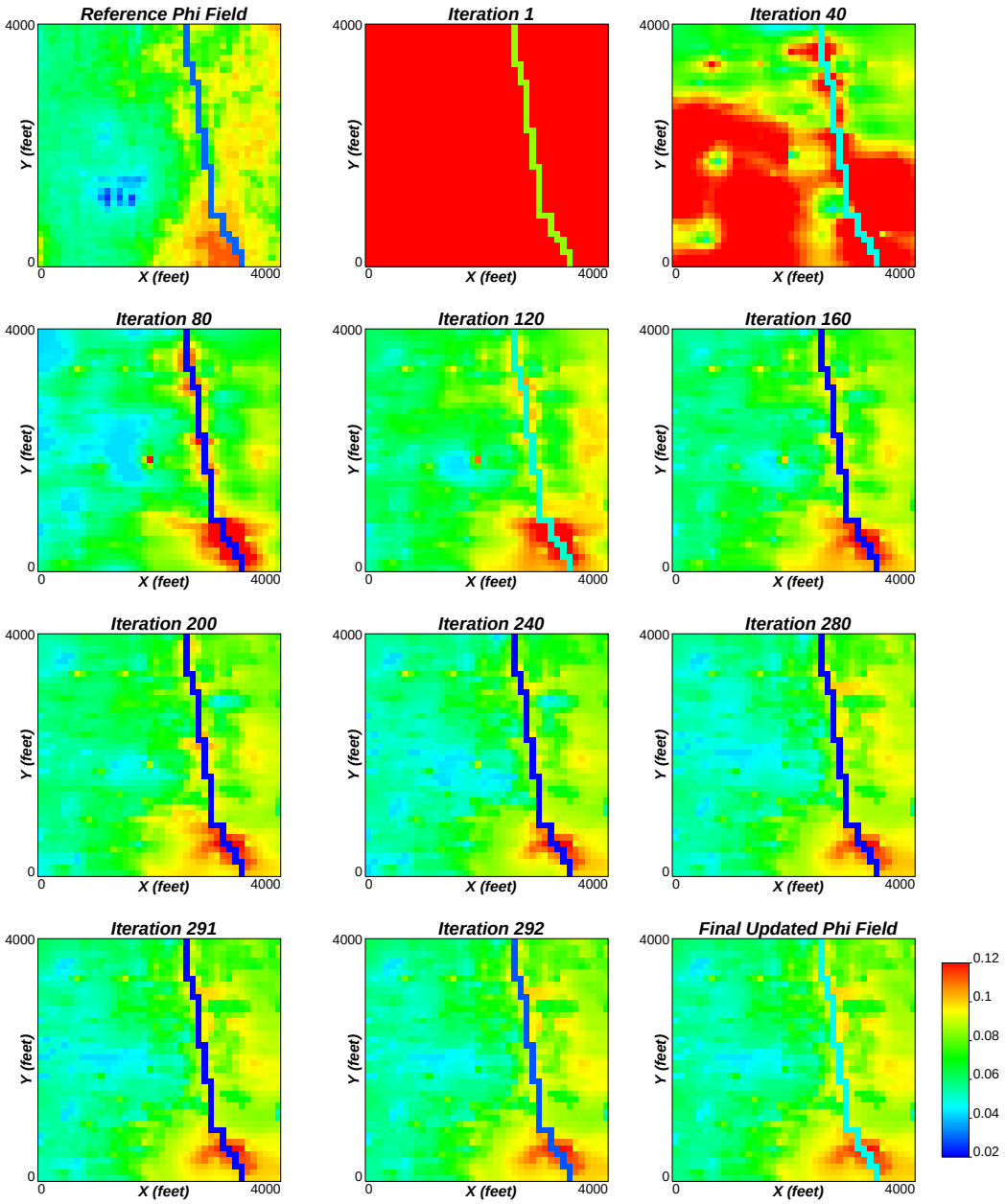

Figure 59: Updated ϕ fields at some outer iterations: 3 Well Case.

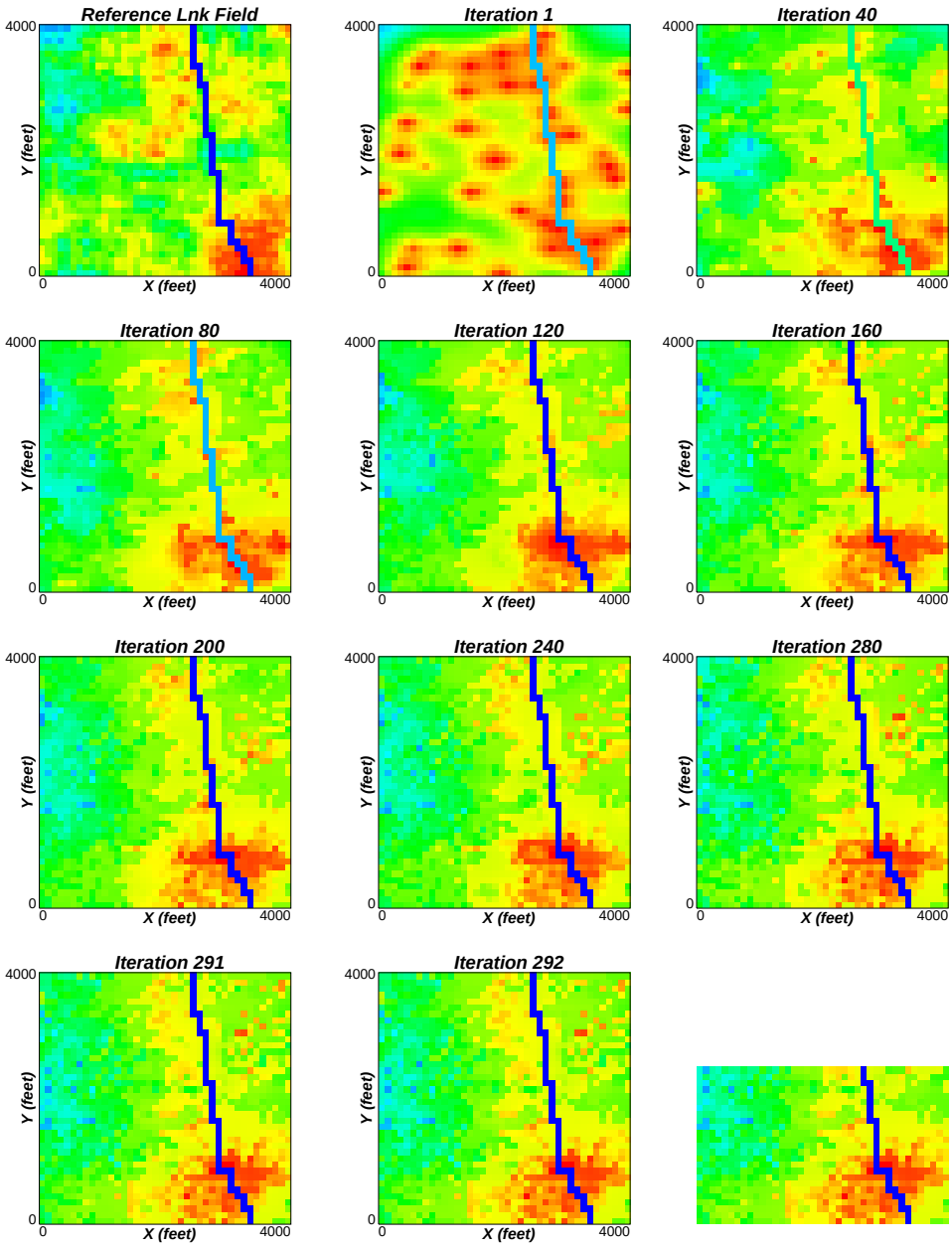

Figure 60: Updated $\ln(k)$ fields at some outer iterations: 3 Well Case.

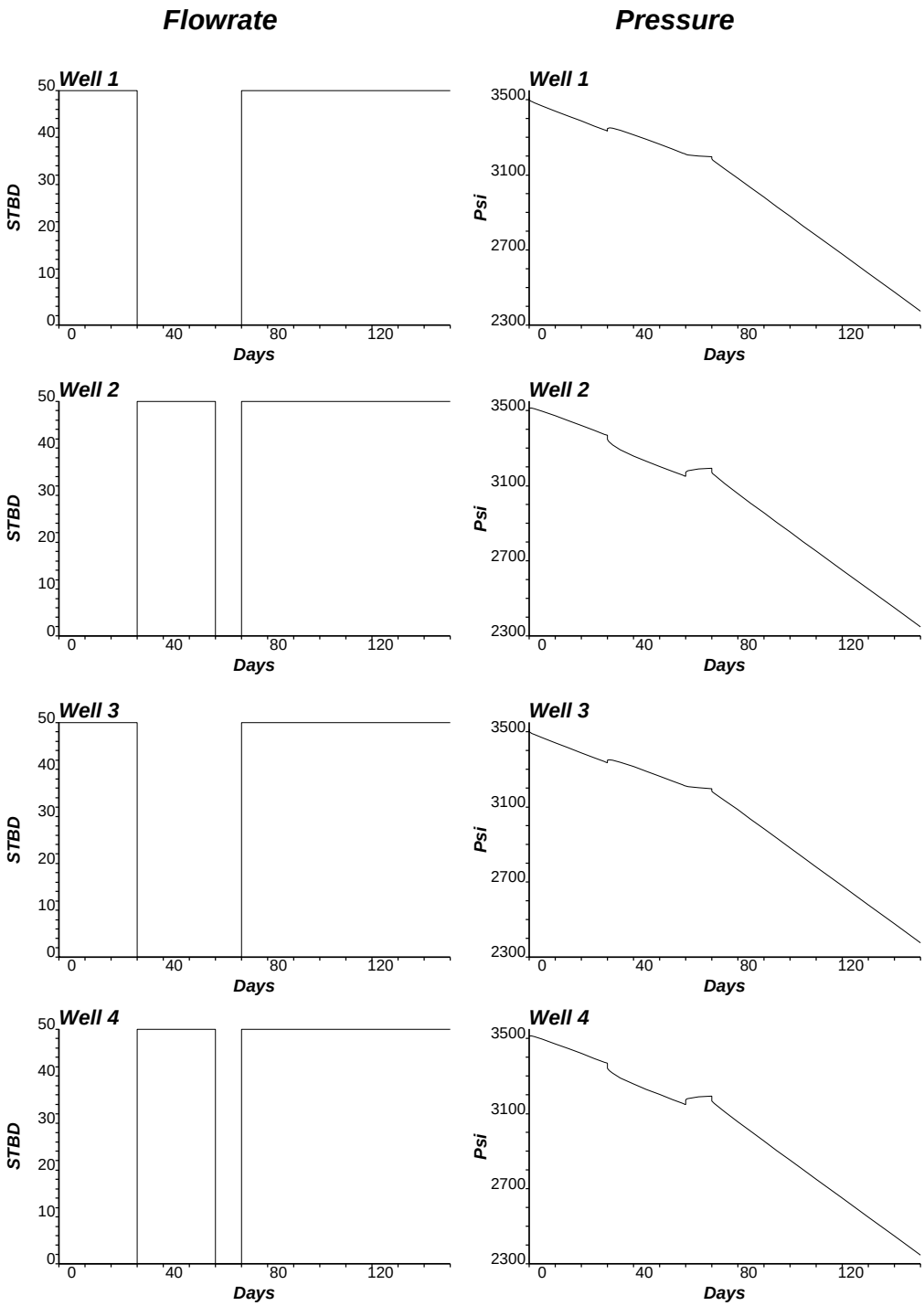

Figure 61: Production data (pressure and flow rates) obtained from the reference field: 4 Well Case.

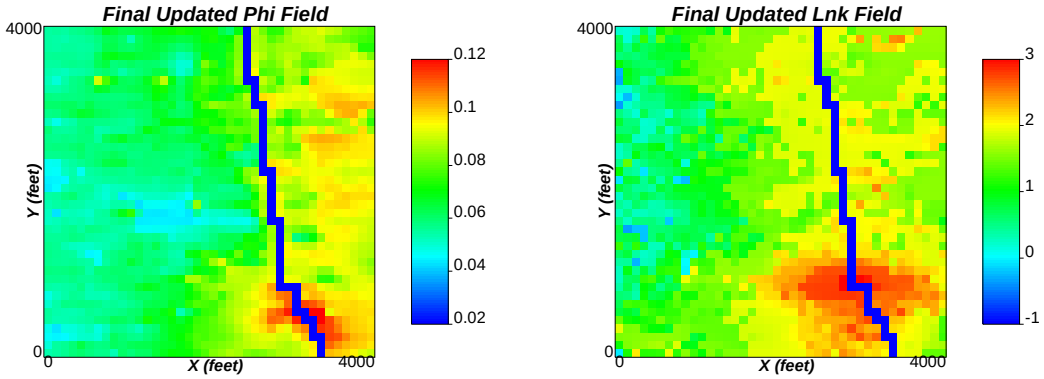

Figure 62: Updated ϕ and $\ln(k)$ fields: 4 Well Case.

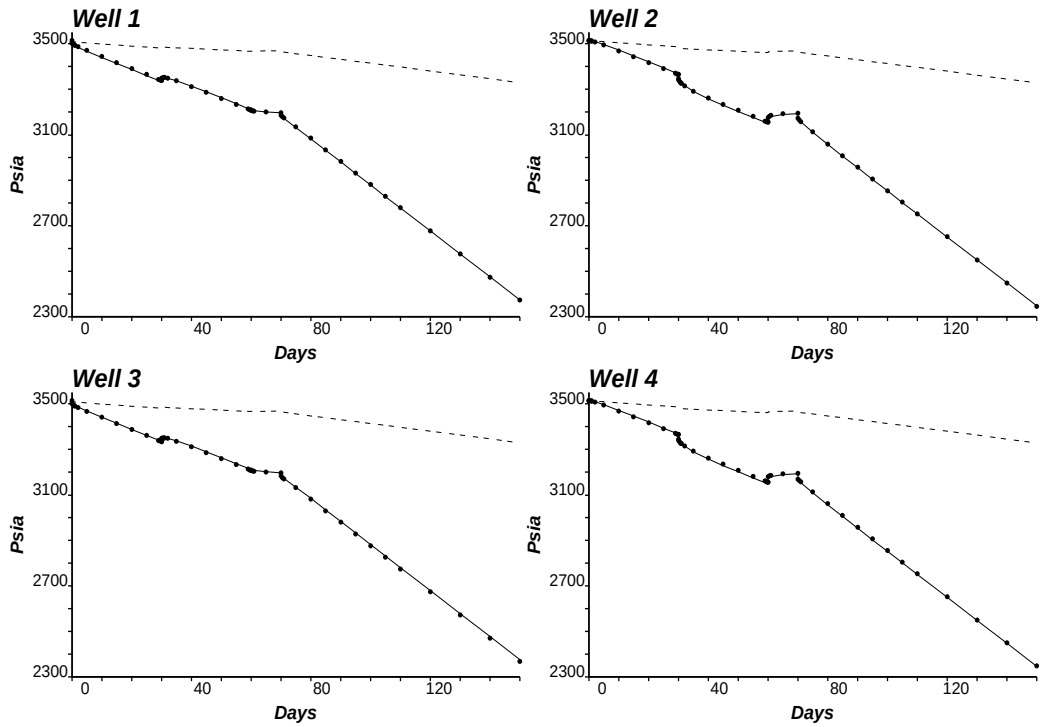

Figure 63: Pressure responses computed from initial (dashed lines) and updated (bullets) ϕ and $\ln(k)$ fields with the true data (solid lines): 4 Well Case.

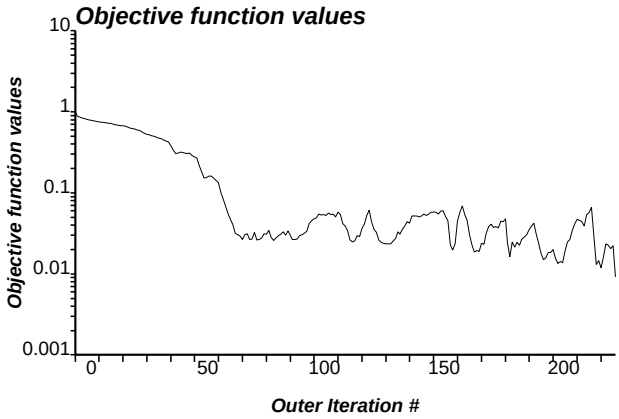

Figure 64: Objective function values of the inversion process: 4 Well Case.

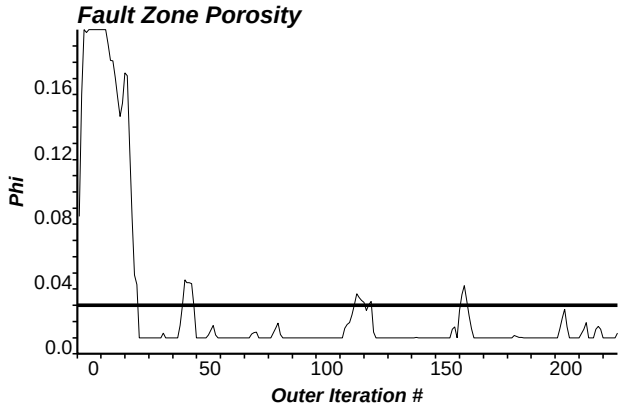

Figure 65: Fault zone ϕ values for each outer iteration: 4 Well Case. (Reference value: thicker horizontal line)

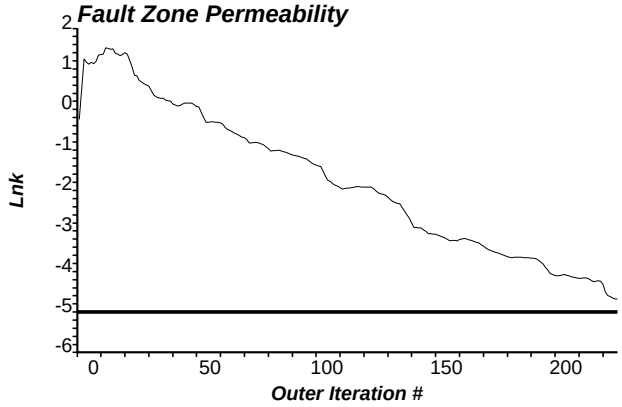

Figure 66: Fault zone $\ln(k)$ values for each outer iteration: 4 Well Case. (Reference value: thicker horizontal line)

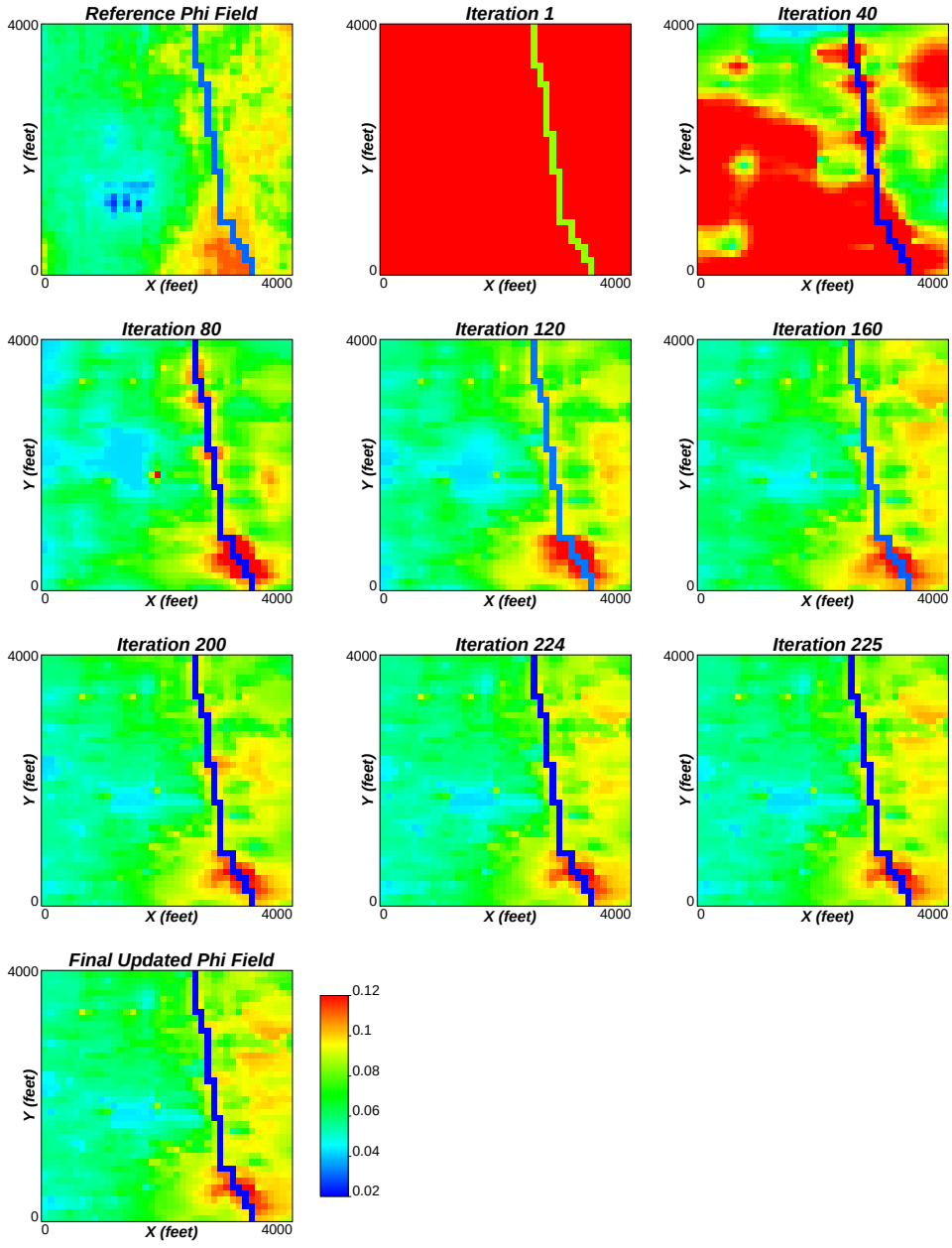

Figure 67: Updated ϕ fields at some outer iterations: 4 Well Case.

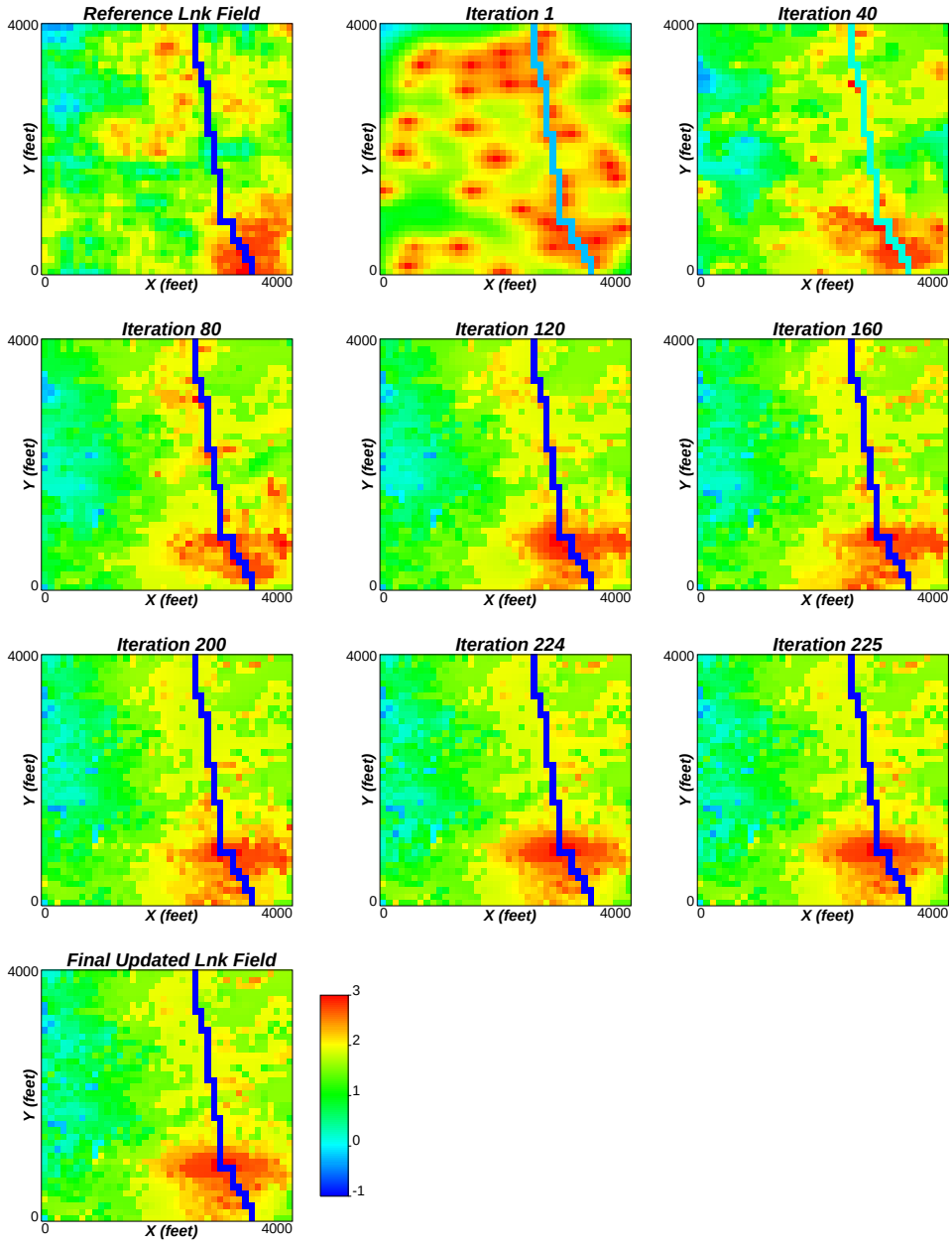

Figure 68: Updated $\ln(k)$ fields at some outer iterations: 4 Well Case.

Conclusion

In this paper, we discussed our algorithm for fault property inversion and its capability to capture reservoir heterogeneity as well as fault properties. The inversion outcomes using different exercises discussed are remarkable. It appears that in the initial outer iterations reservoir heterogeneity is resolved. Information for fault properties are captured at the later outer iterations. This is evident from the objective function value curves for all the above exercises. Inversion of reservoir properties are better resolved for sealing fault when the production data have interference information as in Case A. Inversion outcomes are robust to number of master points or a priori fault zone information. Amount of production data may not affect the inversion results as long as the interference information is available.

References

[1] Z. A. Reza, X.-H. Wen, and C. V. Deutsch. Simultaneous inversion of porosity and permeability using multiple well production data. In *Report 4*, Edmonton, Canada, March 2002. Center for Computational Geostatistics.